Bulletin of Earthquake Engineering (2024) 22:951–995
https://doi.org/10.1007/s10518-023-01792-x

ORIGINAL ARTICLE

Simplified pushover-based seismic loss assessment for existing infilled frame structures

Al Mouayed Bellah Nafeh[1] · **Gerard J. O'Reilly**[1]

Received: 6 June 2023 / Accepted: 27 September 2023 / Published online: 30 October 2023
© The Author(s), under exclusive licence to Springer Nature B.V. 2023

Abstract
Loss assessment is becoming a more familiar instrument in the seismic performance assessment of existing structures. Different approaches exist with varying degrees of complexity. The most notable is the component-based approach implemented within the FEMA P-58 guidelines. Despite recent research developments, practitioners must be provided with tools to conduct building-specific loss assessments simply and accurately. A simplified alternative to computationally intense component-based loss assessment is via storey-loss functions (SLFs). They reduce computational effort by describing a building typology's expected repair costs directly as a function of structural demands typically available to engineers, circumventing many steps of damage state and repair cost estimation for each individual damageable element in the structure. This study presents a pushover-based approach to estimate economic losses intended for practical application. It is implemented within a previously defined framework for simplified pushover-based seismic risk estimation via seismic hazard and vulnerability approximations. This additional simplification of direct losses utilises SLFs with structural response parameters like peak storey drift and peak floor acceleration. The steps required to apply the proposed approach are demonstrated via a case study application to infilled reinforced concrete frame structures. The method's accuracy is appraised via a comparison with other simplified loss assessment methodologies currently available. It is seen that when taking the more rigorous component-based approach as a benchmark, the proposed approach exhibits excellent accuracy and robustness compared to existing methodologies of this sort, paving the way as a candidate to adopt in future codes and guidelines.

Keywords PBEE · Seismic loss · Assessment · Pushover · Storey-loss function

✉ Gerard J. O'Reilly
gerard.oreilly@iusspavia.it

Al Mouayed Bellah Nafeh
mouayed.nafeh@iusspavia.it

[1] Centre for Training and Research on Reduction of Seismic Risk (ROSE Centre), Scuola Universitaria Superiore IUSS Pavia, Palazzo del Broletto, Piazza della Vittoria 15, 27100 Pavia, Italy

1 Introduction

Recent advances in earthquake engineering knowledge (e.g., seismic hazard, structural behaviour), and the increased public concern for earthquake-induced monetary losses have been catalysts for developing improved seismic performance assessment frameworks. The past years have witnessed a substantial increase in seismic knowledge (i.e., design standards and assessment guidelines) also aided by the progress in numerical simulation capabilities, experimental testing, and empirical observations following earthquake events. Consequently, efforts to improve the performance quantification of structures in terms of more accurate metrics have been developed. Most notably for the characterisation of seismic risk, the Pacific Earthquake Engineering Research Center's performance-based earthquake engineering (PEER-PBEE) methodology (Cornell et al. 2002; Cornell and Krawinkler 2000) represents a widely-adopted framework among decision-makers and practitioners. It generally utilises three decision variables (DVs): economic losses, downtime, and fatalities, although more recent extensions via the REDi guidelines (Almufti and Willford 2013) or Molina Hutt et al. (Molina Hutt et al. 2022) have looked to incorporate concepts like robustness and rapidity when considering post-earthquake functionality. The classic PEER-PBEE approach consists of four stages of analysis:

$$\lambda[DV > x] = \iiint P[DV > x|DM]f[DM|EDP]f[EDP|IM]|dH(IM)dEDPdDM \quad (1)$$

where $\lambda[DV > x]$ is the annual rate of DV exceeding a given threshold x, DM is the damage measure representing the discrete damage states of the components of any building or facility; EDP is the engineering demand parameter such as peak storey drift (PSD) or peak floor acceleration (PFA), and IM is the ground-motion intensity measure. Additionally, $dH(IM)$ is the ground-motion hazard curve's local derivative and the $f[c|d]$ terms are conditional probability distribution functions for c given d.

Design standards such as Eurocode 8 (EC8) (European Standard 2004) and New Zealand's NZS 1170.5 (NZS 1170.5:2004 2004) typically evaluate the performance of structures at discrete hazard levels. In contrast, PEER-PBEE quantifies performance via a fully probabilistic framework accounting for uncertainties related to hazard, structural response, damage estimation, and economic loss quantification. However, due to its probabilistic nature and computationally expensive application, it remains popular within the academic community and specialised studies and reports, such as FEMA P-58 (FEMA 2012) and the CNR guidelines (CNR 2014).

A simplified alternative to the computationally demanding PEER-PBEE approach for building-specific loss estimation was proposed by Ramirez and Miranda (Ramirez and Miranda 2009), where the EDP and expected repair costs were directly related, essentially condensing the first two terms inside the integral of (1 to $f[DV|EDP] = P[DV|DM]f[DM|EDP]$. These functions describe the expected repair costs at a storey level with a predefined inventory of damageable components and were thus termed storey-loss functions (SLFs). While SLFs can be challenging to assemble due to the required data and difficulty in obtaining it for every single damageable component, they offer an expedited solution to estimate losses in structures where the general composition of building components is known. For example, FEMA P-58–2 (FEMA 2012a) offers simplified tools such as the "Normative Quantity Estimation Tool" to provide users with approximate quantities of non-structural components typically present in buildings given the occupancy type and floor plan area. It should also

be noted that the advancements in BIM modelling (Welch et al. 2014a; Alirezaei et al. 2016; Perrone and Filiatrault 2017) can also be considered a valuable source of such detailed information. Additionally, generalised SLFs based on normalised quantities can be easily adapted, further minimising the computational effort required by component-based approaches. Studies such as Silva et al. (Silva et al. 2020a) and Papadopoulos et al. (Papadopoulos et al. 2019) have been implemented for steel buildings and office typologies in Europe, respectively. However, SLF options for reinforced concrete (RC) buildings are generally lacking, especially for contexts other than the US, and the need to develop such SLFs remains a priority.

Despite the different loss assessment methodologies which have emerged in recent years to enable seismic risk assessment, there is still a need to provide engineers with tools to perform building-specific loss assessment and ultimately enable more informed decision-making at a practitioner level. This is primarily due to comprehensive probabilistic methodologies perhaps appearing overly complex or excessively detailed for practical decision-making. One merely needs to apply the component-based approach of FEMA P-58 FEMA (2012b) to understand the level of detail required, such as numerical models detailed enough to capture all possible inelastic mechanisms, ground motion selection for non-linear time history analyses (NLTHA), damageable inventories with quantities, fragility functions and expected repair costs for every single damageable element, among other steps. FEMA P-58 has done immense work in providing a good starting point on many of these issues, with the PELICUN (Zsarnóczay and Deierlein 2020) and SP3 (Haselton-Baker Risk Group2020) softwares also making further enhancements to the computational tools available. Still, each is typically focused on the US context. Other studies (Vecchio et al. 2018) in Europe have repeatedly highlighted the need to develop alternatives that are more representative of the local context and others (Silva et al. 2020b) have proposed means of adapting the FEMA P-58 database, for example. This is further underlined by the Italian government's decision Ministero delle Infrastrutture e dei Trasporti (2017) to use seismic loss estimates to quantify seismic risk and adopt it as a parameter to offer financial incentives to building owners willing to upgrade and retrofit.

To address these needs, this study proposes a simple and practical framework to estimate direct economic losses in structures based on static pushover (SPO) analysis results. It exploits the SLF-based concept by (Ramirez and Miranda 2009) in tandem with the recent toolbox developed by (Shahnazaryan et al. 2021) to create user-specific SLFs. Furthermore, recent studies on loss estimation (Perrone et al. 2022; Sullivan 2016) underline the need to develop SLFs encompassing a wide range of building characteristics (e.g., building occupancy type). This study first illustrates the feasibility of adopting SLFs as an alternative to component-based approaches for seismic loss assessment through a case study comparison. Second, a generic set of component-based approach-compatible SLFs for infilled RC building typologies representative of those found in Italy is derived and presented. The generalised SLFs are derived considering specific storey typologies and account for potential differences in damageable inventories observed through literature review and professional consultation. These include ground storey levels, typical storeys throughout the remaining building height, pilotis ground storeys, and roof levels, where the damageable elements would be expected to differ significantly. These generalised SLFs are formalised into a pushover-based seismic loss assessment methodology, termed *PB-Loss* herein, with case study examples illustrated. *PB-Loss* is then validated using an extensive database of infilled RC structures designed for different temporal periods in Italy (e.g., gravity-load designed). Its accuracy and improvement compared to other simplified methodologies available in the literature are appraised.

2 Component- versus SLF-based loss assessment

A comparative assessment was conducted to illustrate the potential benefit of using an SLF-based instead of the component-based approach outlined in FEMA P-58. To do this, three case study buildings hypothetically located in L'Aquila, Italy were considered. The plan layout of the case study building is illustrated in Fig. 1. It is a three-storey structure are representative of pre-1970s Italian residential buildings that were designed to resist gravity loads only using the allowable stress method (i.e., prior to the introduction of seismic guidelines) and is assumed regular in plan. Column sections are 25 × 25 cm with ϕ16 longitudinal rebars and transverse reinforcement of ϕ6 stirrups at 150 mm each. Drop beams of 50 × 30 cm spanning in one direction only were considered with ϕ16 longitudinal rebars and transverse reinforcement of ϕ6 stirrups at 200 mm each. Aq42 smooth rebars with an allowable stress of 140 MPa and 15 MPa concrete were used to reflect on the sub-standard construction practice adopted at the time. The buildings correspond to the identification tag GLD-A-3 in an existing database of archetypes available online (Nafeh and O'Reilly 2022). The difference between the three cases considered here was the consideration of masonry infills (i.e., bare, pilotis, and fully infilled). Further details on their design and numerical modelling are provided by (Nafeh and O'Reilly 2022).

NLTHA were conducted to quantify the relationship between structural demand and seismic intensity. Probabilistic seismic hazard analysis (PSHA) was carried out using the OpenQuake engine to characterise the site hazard, adopting average spectral acceleration, Sa_{avg}, as the IM. Hazard-consistent records were selected from the NGA-West2 database with the conditional spectrum method (Lin et al. 2013) using the EzGM tool developed by (Ozsarac 2022). Multiple-stripe analysis (MSA) was conducted for nine intensities spanning return periods $T_R = 22 - 4975$ years to characterise the structural response from initial damage right up to global structural instability or collapse.

Once the structural typology has been established, the list of damageable components, or simply the damageable inventory, is needed for loss assessment purposes. To do this, three performance groups (PGs) comprising structural and non-structural components, and building contents likely to be damaged and contribute to the economic loss were identified. To define this inventory, fragility and consequence functions may be adapted from



Fig. 1 Plan layout of the case study building

the FEMA P-58 database or other similar sources. The damageable inventory was selected from Tables 3 and 4 of Appendix 1, where only the variability in masonry infill panels was considered. Here, component-based loss assessment was carried out using the PACT software (FEMA 2012b), where each record's EDPs (i.e., PSDs and PFAs) were used.

To apply the SLF-based approach, the same damageable inventory was considered. Depending on the components' sensitivity to a specific EDP, components were then classified into PGs, meaning those within a PG were assessed together for a mutual demand level and consequent losses were summed to estimate the PG's SLF. Then, a Monte-Carlo simulation was carried out as described in (Shahnazaryan et al. 2021) where damage and repair costs were sampled for each component of the PG and each cost was summed to quantify the PG total loss for a given EDP. The SLFs were then derived through regression analysis on the normalised repair costs for a given EDP and a Weibull function was considered to fit the observed data. For drift-sensitive components, two sets of SLFs were derived for the corresponding elements and accounted for losses in the two principal directions. For acceleration-sensitive components, a single set of SLFs was derived, given the non-directionality of these elements. The entire assembly of the SLFs used herein was developed using the SLF toolbox of (Shahnazaryan et al. 2021). It is worth mentioning that following MSA, the median PSD and PFA demands were used for the SLF-based approach. As such, the comparison will be purely in terms of SLFs' ability to quantify losses with respect to component-based methods, and not be influenced by other factors.

The results of the case study comparison are shown in Fig. 2 in terms of their vulnerability curves (i.e., expected loss ratio versus intensity, $E[L_T|IM = im]$) and loss curves (i.e., the annual frequency of exceedance, $H(IM)$, versus expected loss ratio). Scrutinising the estimates of losses obtained from both the component-based and SLF-based methods, Fig. 2a shows a very good match for the buildings analysed. This is seen through the close matching of the vulnerability curves estimated following both approaches. Small differences observed were found to be due to the difficulty in ensuring an exact fitting of the regression functional form adopted within the SLF toolbox of (Shahnazaryan et al. 2021). This is particularly notable at low intensities and could be overcome by developing more advanced fitting functions or simply using the tabulated output of the SLF toolbox. This good matching of the SLF-based method is further confirmed via the loss curves illustrated

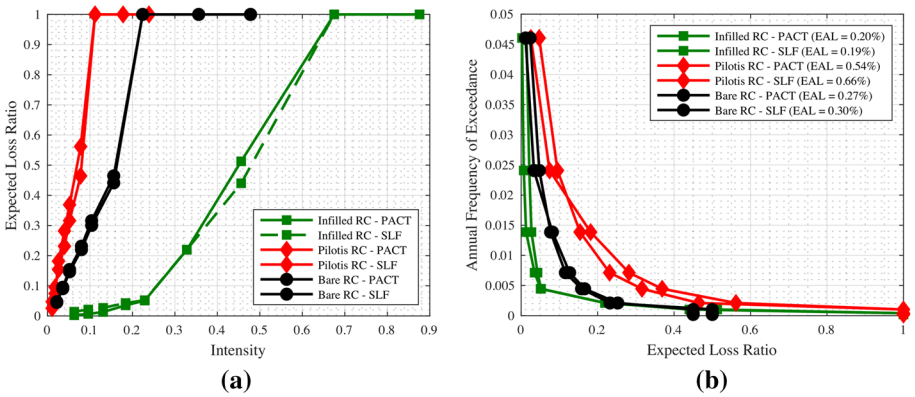


Fig. 2 Comparison of the results obtained from the component-based (PACT) and the SLF-based approach **a** vulnerability curves and **b** loss curves

in Fig. 2b and the estimates of the expected annual loss (EAL). Here the trends of losses are well-represented and the differences between the two approaches were minimal when expressed in terms of the EAL values noted in Fig. 2 for the infilled, pilotis and bare RC buildings.

Overall, this shows that the outputs obtained from the comprehensive component-based loss assessment described in FEMA P-58 and the simplified SLF-based approach yield similar results regarding vulnerability curves and annualised losses. Hence, the following sections will seek to build on this finding and describe a simplified loss assessment methodology using pushover analysis as its input.

3 Proposed methodology for simplified seismic loss assessment

A simplified pushover-based seismic loss assessment methodology, herein denoted *PB-Loss*, is presented. The method integrates the findings of previous work (Nafeh et al. 2020), denoted *PB-Risk* that evaluates the seismic performance of a single building via estimation of structural vulnerability from just a pushover analysis. *PB-Loss* expands and develops this *PB-Risk* methodology. It provides practitioners with a simple way of estimating the monetary losses expected in a building's structural and non-structural components also from just a pushover analysis. Having characterised the seismic hazard and vulnerability components, the seismic loss can be evaluated from a suitable set of SLFs tailored specifically for infilled RC typologies. This section outlines the general steps of the proposed *PB-Loss* framework. Section 4 describes a generalised set of SLFs that can be used as part of the methodology, which are then applied and appraised in Sect. 5. A practical step-by-step example application of *PB-Loss* is also given in Appendix 2.

With reference to Fig. 3, four main modules are: (1) hazard; (2) vulnerability, which are used to compute either (3) risk (i.e., *PB-Risk* (Nafeh and O'Reilly 2023)); or (4) loss (i.e., *PB-Loss*, presented here).

3.1 Seismic hazard assessment and intensity measure identification

1. Perform PSHA to determine the annual rate of exceeding a specified ground motion intensity, $H(IM)$, or simply adopt the results of a suitable seismic hazard study. In *PB-Loss*, the mean hazard curves associated with the average spectral acceleration, $Sa_{avg}(T^*)$, where T^* is the anchoring period of the Sa_{avg} definition described in (Nafeh and O'Reilly 2023) and the peak ground acceleration, (PGA), are required (Fig. 4). $Sa_{avg}(T^*)$ is calculated as per the definition of (Eads et al. 2015) as such:

$$Sa_{avg} = \left(\prod_{i=1}^{N} Sa\left(c_i T^*\right) \right)^{1/N} \tag{2}$$

where c_i represent $N = 10$ number coefficients in the range of 0.2 and 3.0 as proposed by (O'Reilly 2021) to account for period-elongation effects in non-ductile infilled RC frame buildings;

2. From each hazard curve (i.e., $Sa_{\text{avg}}(T^*)$ or PGA), identify the intensity levels corresponding to the code-based return periods, T_R, (denoted herein as *im*) and subsequently their annual exceedance rates, $H(IM = im)$, where $H(IM) = 1/T_R$ (as per Fig. 4). The Italian national code (NTC 2018) identifies four return periods at which building limit states

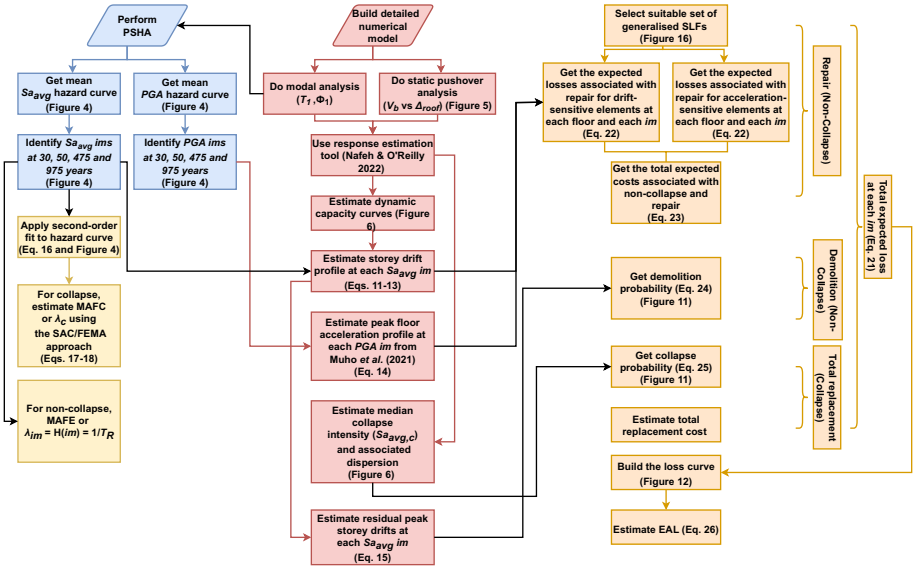


Fig. 3 Overview of the proposed *PB-Loss* methodology

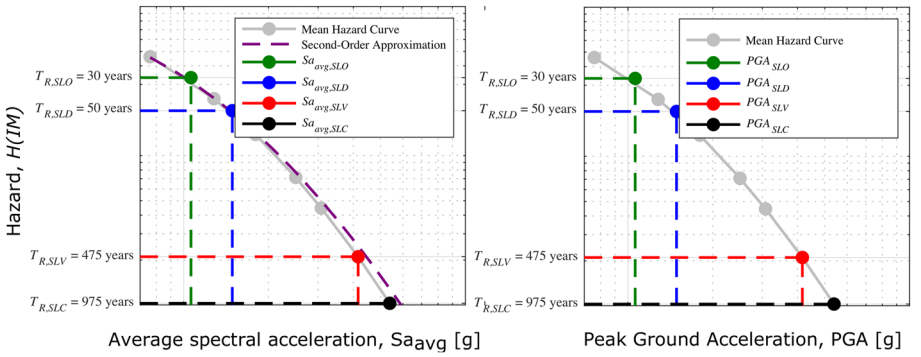


Fig. 4 Mean Sa_{avg} and *PGA* hazard curves for a particular case study site with the intensity measure levels at the identified NTC2018 code-based return periods

(LSs) are checked, and are listed herein in Table 1 for regular structures since T_R values depend on the importance class of a given structure.

Table 1 Description of the NTC2018 limit states

Limit State	Return Period, T_R (years)	Annual Rate of Exceedance, $H(IM) = 1/T_R$
Operational—*Stato Limite di Operatività* (SLO)	30	0.033
Damage Control—*Stato Limite di Danno* (SLD)	50	0.020
Life-Safety—*Stato Limite di Salvaguardia della Vita* (SLV)	475	0.0021
Collapse Prevention—*Stato Limite di Prevenzione del Collasso* (SLC)	975	0.0010

3.2 Seismic vulnerability assessment: non-collapse and collapse capacities

To characterise the vulnerability, the median seismic response is estimated at each of the intensities, *im*, identified on the hazard curve. Furthermore, the collapse fragility function parameters, namely the median collapse intensity and the associated dispersion, are also identified.

To do this, the response estimation tool developed by (Nafeh and O'Reilly 2022) is employed for infilled RC frames, although other tools (e.g., (Vamvatsikos and Cornell 2006; Guerrini et al. 2017)) may be utilised for other typologies. It uses response parameters obtained via a pushover analysis, and the modal properties of the structure to empirically estimate the dynamic response of the structure, as follows:

1. Build a sufficiently detailed numerical model of the structure, accounting for all pertinent mechanisms and failure modes;
2. Perform a modal analysis to obtain the normalised first-mode shape ordinates at each floor i, $\Phi_{1,i}$;
3. Perform an SPO analysis in both principal directions of the building to characterise the lateral response in terms of nominal base shear, V_b, and roof displacement, Δ_{roof};
4. Multi-linearise the SPO curve to indicate the onset and end of each response branch (i.e., elastic, hardening, post-capping or softening and residual strength plateau) as illustrated in Fig. 5.
5. The equivalent single-degree-of-freedom (SDOF) properties, expressed in terms of equivalent base shear, V_b^*, and displacement, Δ^*, are determined as follows:

$$V_b^* = \frac{V_b}{\Gamma} \tag{3}$$

$$\Delta^* = \frac{\Delta_{roof}}{\Gamma} \tag{4}$$

$$\Gamma = \frac{\sum_i m_i \Phi_{1,i}}{\sum_i m_i \Phi_{1,i}^2} \tag{5}$$

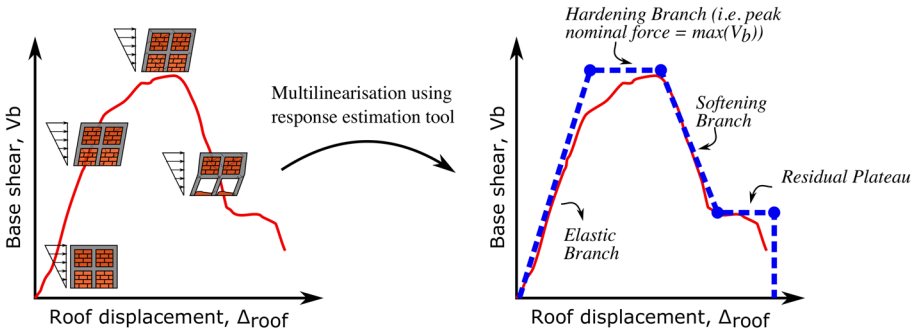


Fig. 5 Multi-linearisation of static pushover curve based on onset and end of response branches (steps 3–4)

where Γ is the first-mode transformation factor computed via Eq. (5) assuming a first-mode based non-torsional behaviour of the building, m^* and T^* are the effective mass and period of the equivalent SDOF system; m_i is the mass at floor i of the multi-degree-of-freedom (MDOF) system;

6. Using the response evaluation tool for infilled RC frames (Nafeh and O'Reilly 2022), the seismic demand-intensity model is calculated for the structure's equivalent SDOF in both principal directions of the building. It is expressed in terms of a dynamic strength ratio, ρ, for a given ductility demand, μ. It estimates both the collapse and non-collapse performance of the equivalent SDOF structure (Fig. 6). The dynamic strength ratio, ρ and ductility, μ are related via a bilinear demand-intensity model previously derived in (Nafeh and O'Reilly 2022) which adopts a combination of two linear models in the log-space described by:

$$\mu \leq 1, \rho = \exp\left(a_1 \ln(\mu) + b_1\right); a_1 = 1 \text{ and } b_1 = b_2 \tag{6}$$

$$\mu > 1, \rho = \exp\left(a_2 \ln(\mu) + b_2\right); \tag{7}$$

where a_2 and b_2 are coefficients obtained via two-step regression expressed as a function of the fundamental period of the structure and response parameters characterising the structural system.

7. The dynamic strength ratio, ρ, is similar to the strength ratio, R, adopted in EC8. However, ρ represents the ratio between the median average spectral acceleration, $Sa_{avg}{}^*$ (as opposed to $Sa(T_1)$) and the yield spectral acceleration of the equivalent SDOF system, Sa_y^*, indicated in Eq. (10).

$$\rho = \frac{Sa_{avg}^*}{Sa_y^*} \tag{8}$$

As such, (8) can be rewritten to calculate the median intensity ($\widehat{Sa}_{avg}$) required for the MDOF system to exceed a given ductility demand is computed from the tool as:

$$\widehat{Sa}_{avg} = \hat{\rho} Sa_y^* \Gamma \tag{9}$$

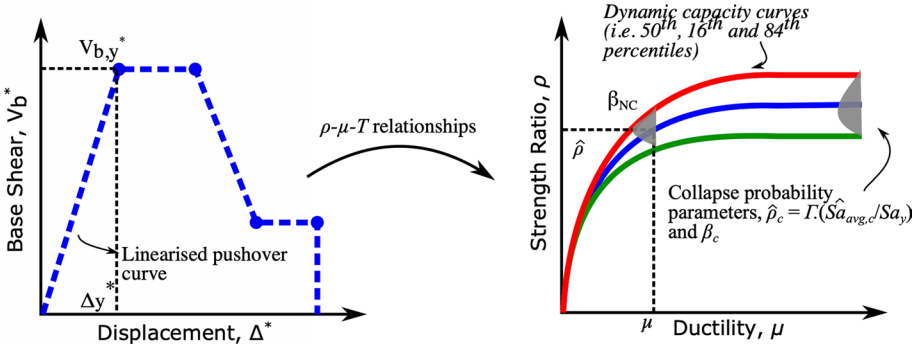


Fig. 6 Estimation of dynamic response via ρ-μ-T relationships (Steps 5–8)

$$Sa_y^* = \frac{4\pi\Delta_y^*}{T^{*2}g} = \frac{V_{b,y}^*}{m^*g} \tag{10}$$

where $V_{b,y}^*$ and Δ_y^* are the base shear and displacement at yield of the equivalent SDOF system;

For collapse, the median seismic collapse intensity, $\widehat{Sa}_{avg,C}$, and the associated dispersion, β_C are identified directly by the response estimation tool;

The response estimation tool for carrying out single-building vulnerability assessment can be accessed here: https://github.com/gerardjoreilly/Infilled-RC-Building-Response-Estimation.

The main limitation of the pushover-based approach is that the ρ-μ-T relationships were derived based on extensive analysis on representative SDOF systems. This means that it is applicable for structures with a first-mode dominated response and as such, torsional effects were not accounted for. This translates as a limitation of the ρ-μ-T when applied for example, to irregular structures where the center of mass and stiffness do not coincide. Moreover, a limitation regarding the derived MDOF capacity curves is the additional record-to-record variability displayed due to the influence of higher modes (Vamvatsikos and Cornell 2005) which SDOF systems cannot account properly for. To address this issue, (Baltzopoulos et al. 2017), for example, derived empirical rules which were implemented at the nominal yield point and subsequently extended across the entire range of response. Furthermore, this limitation extends to the estimation of PFA demands which are related to the contribution of higher modes. The pushover-based method presented in this study does not account implicitly for higher modes effects. For this reason, other methods existing in the literature (and described in detail in subsequent sections) were scrutinised and implemented in the proposed pushover-based approach to abridge this issue for the estimation of PFA demands.

3.3 Seismic demand estimation

To evaluate monetary losses, the outcome of the simplified vulnerability assessment carried out in the previous section is necessary to identify a relationship between each *im* and the total expected losses. This relationship is represented by the structural response parameters or the EDP demand. The EDP demand is characterised via the PSD and PFA quantities, depending on the PG under investigation. Moreover, another component of seismic loss assessment is the residual peak storey drift (RPSD). The influence of residual drifts is related to the possibility of a building requiring demolition due to excessive permanent lateral deformation. Ramirez and Miranda (Ramirez and Miranda 2012), for example, have indicated that economic losses at moderate levels of ground-shaking were significantly driven by losses due to residual drifts. In the subsequent sub-sections, simplified approaches to estimate PSD, PFA and RPSD quantities are described.

3.3.1 Peak storey drifts

The PSD demands are a notable contributor to the damage of drift-sensitive structural and non-structural components. The distribution of PSD along a building's height is not necessarily consistent and uniform, where deformation may tend to concentrate at specific floors based on the building's structural characteristics and inelastic mechanisms. For

the accurate loss assessment of drift-sensitive components, it is necessary to accurately identify where in the building this maximum response occurs because it directly relates to structural damage. Different procedures for the estimation of peak storey drift profiles in multi-storey buildings exists with different degrees of complexity. For example, (Khaloo and Khosravi 2008) conducted an extensive investigation on the lateral structural response under pulse-type ground motions in near-field earthquakes, using a multi-modal continuous beam model. Similarly, (Neam and Taghikhany 2016) proposed prediction equations for interstory drift spectrum considering near-fault ground-motions whereas (Eroğlu and Akkar 2011) proposed storey-dependent lateral stiffness coefficients for the estimation of peak storey drift values across the building height for frame-type buildings based on the model by (Heidebrecht and Stafford 1973). Furthermore, (Miranda and Akkar 2006) derived the inter-story drift spectrum for buildings subjected to earthquake ground motions and Alonso-Rodríguez and Miranda (Alonso-Rodríguez and Miranda 2016) examined a continuous beam model that incorporates a shear beam with a variable stiffness following a parabolic pattern and a Bernoulli beam with a fourth-order flexural stiffness. In a more recent investigation, Alonso-Rodríguez and Tsavdaridis (Alirezaei et al. 2016) explored how rotational inertia influences the structural response of the continuous shear–flexural beam model. Moreover, Miranda and Reyes (Miranda and Reyes 2002) presented an approximate method to estimate the lateral drifts in multistorey buildings with non-uniform stiffness responding subjected to earthquake ground motions based on an equivalent continuum structure (i.e. combination of flexure and shear cantilever beams). (Lai et al. 2021) derived an analytical solution to estimate the interstory drift for high-rise buildings using a coupled flexural-shear model with mass and stiffness discontinuities across the height. Additionally, (Akkar et al. 2005) proposed a procedure to estimate the local displacement demands in regular frame-type structures subjected to near-fault ground motions. However, most of these procedures require a more in-depth characterisation of local component behaviour and/or information regarding seismicity or time-histories. To this end, for the sake of simplicity, the first-mode-based approach (Priestley et al. 2007) was considered and implemented in *PB-Loss* to estimate demand PSD profiles directly from modal analysis in both principal directions due to its simplicity. Its efficiency was demonstrated in Fig. 7 where a comparative assessment was carried out to estimate the PSD demand profiles across the height of two-case study structures in both principal directions. When compared to the results of NLTHA, the first-mode-based demonstrated a reasonable trade-off between accuracy and computational burden.

However, some limitations on the application of the first-mode-based approximation must be noted. First, the approximation demonstrated reasonable robustness when tested for regular (i.e., plan and elevation) structures that are likely to exhibit a shear-type response (i.e. infilled RC frames) and it may not be suitable for adoption in irregular framed buildings. Second, the first-mode-based approximation should be applied to structures responding around the fundamental mode (i.e. 80% mass participation) and other methods should be considered when torsional and higher-modes contribution are expected.

As such, the application of the approximation entails:

1. For each *im*, estimate the roof displacement demand $\Delta_{roof,im}$ for non-collapse via interpolation of the dynamic capacity curves obtained from the response estimation tool (Fig. 8);

$$\Delta_{roof,im} = \mu_{im}\Delta_y^*\Gamma \tag{11}$$

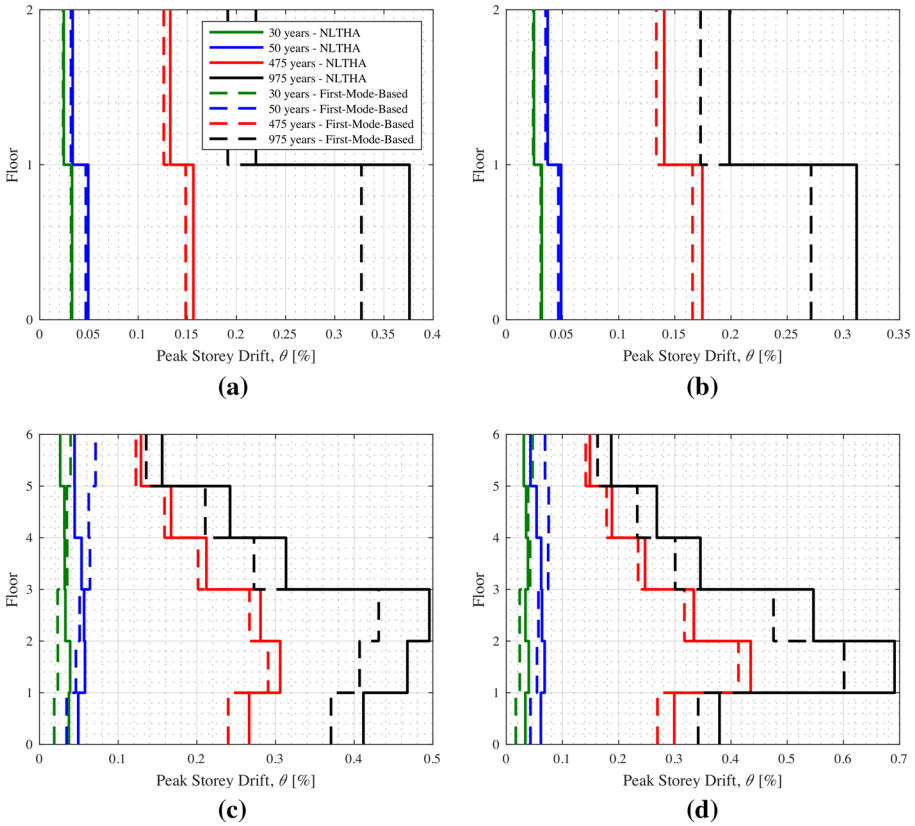


Fig. 7 Comparison of first-mode-based approximation for estimation of peak storey drift demands in (top) 2-storey and (bottom) 6-storey infilled RC frame buildings in both principal directions: **a–c** X, **b–d** Y at 30 years, 50 years, 475 years and 975 years return period intensities

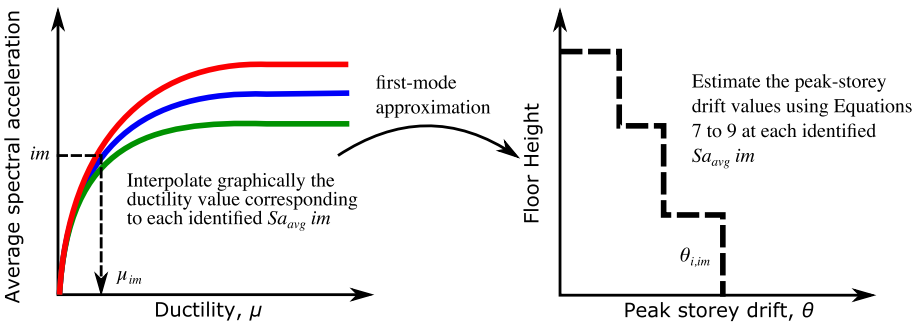


Fig. 8 First-mode approximation for the estimation of the peak-storey drift demand profiles

2. Using a first-mode approximation of the building response, identify the PSD demand profile at each *im* (Fig. 8):

$$\Delta_{i,im} = \Phi_{1,i}\Delta_{roof,im} \tag{12}$$

$$\theta_{i,im} = \frac{\Delta_{i+1,im} - \Delta_{i,im}}{h_i} \tag{13}$$

where $\Delta_{i,im}$ is the displacement at floor i for a particular im; $\Delta_{roof,im}$ is the roof displacement at a given im value of the MDOF system; μ_{im} is the ductility at a given im value $\left(\Delta_{roof,im}/\Delta_{y,roof}\right)$; h_i is the height of storey i and $\theta_{i,im}$ is the drift of storey i at the given im.

3.3.2 Peak floor accelerations

Recent efforts were made to provide practitioners with simplified methods to estimate PFA demand profiles along a building's height at a relatively low computational cost. For example, Welch et al. (Welch et al. 2014b) described a framework where acceleration demands were estimated using empirical relationships implemented in FEMA P-58 (ATC 2011). Other studies such as (Sullivan et al. 2013) and Calvi and Sullivan (Calvi et al. 2014) provide expressions for estimating PFA demands as a function of the inelastic response of the structure. (Vukobratović and Fajfar , 2015, 2016, 2017) proposed a procedure to estimate absolute floor response acceleration spectra for MDOF structures. It requires modal properties and the N2 method (Fajfar 2000) to estimate the response modification factor associated with the ductility demand of the supporting structure. Merino et al. (Merino et al. 2020) proposed a simple correction procedure to predict consistent absolute acceleration demands. O'Reilly and Calvi (O'Reilly and Calvi 2021) describe a method for estimating a peak acceleration whereby a bilinear demand intensity model expressed as a function of the base shear and modal mass is used for first-mode dominated structures. (Miranda and Taghavi, Taghavi and Miranda 2005a, b) presented an approximate method to estimate floor acceleration demands along the structure's height in elastic multi-storey buildings. The method is based on approximating dynamic characteristics represented through equivalent continuum structures consisting of a combination of flexural and shear beams. It requires the calculation of a dimensionless parameter that measures the degree of participation of overall flexural and shear lateral deformations in the building, the ratio of lateral stiffness at roof level to the base of the building, the fundamental period of vibration and a modal damping ratio that characterises the damping in the structure. More recently, (Muho et al. 2021) proposed empirical equations for quantifying maximum PFA response. By assuming an approximate shape for the acceleration amplification factor, Ω, depending on the number of storeys, expressions were calibrated based on extensive parametric NLTHA on a database of infilled frames. Ω could be expressed as a function of the maximum PSD and other key characteristics of the structural system, such as the fundamental period, the ratio of the infill moduli of elasticity along the horizontal and vertical directions and the thickness of the infill panels. These parameters were also observed by (Blasi et al. 2018) to have a significant influence on the PFA demands in infilled RC frames.

To investigate the applicability of the different simplified methodologies discussed above, particularly for infilled RC structures, a case study application on 2 and 6-storey buildings was performed. The 6-storey building was included to investigate the performance of simplified methods when some contribution of higher modes on the PFA

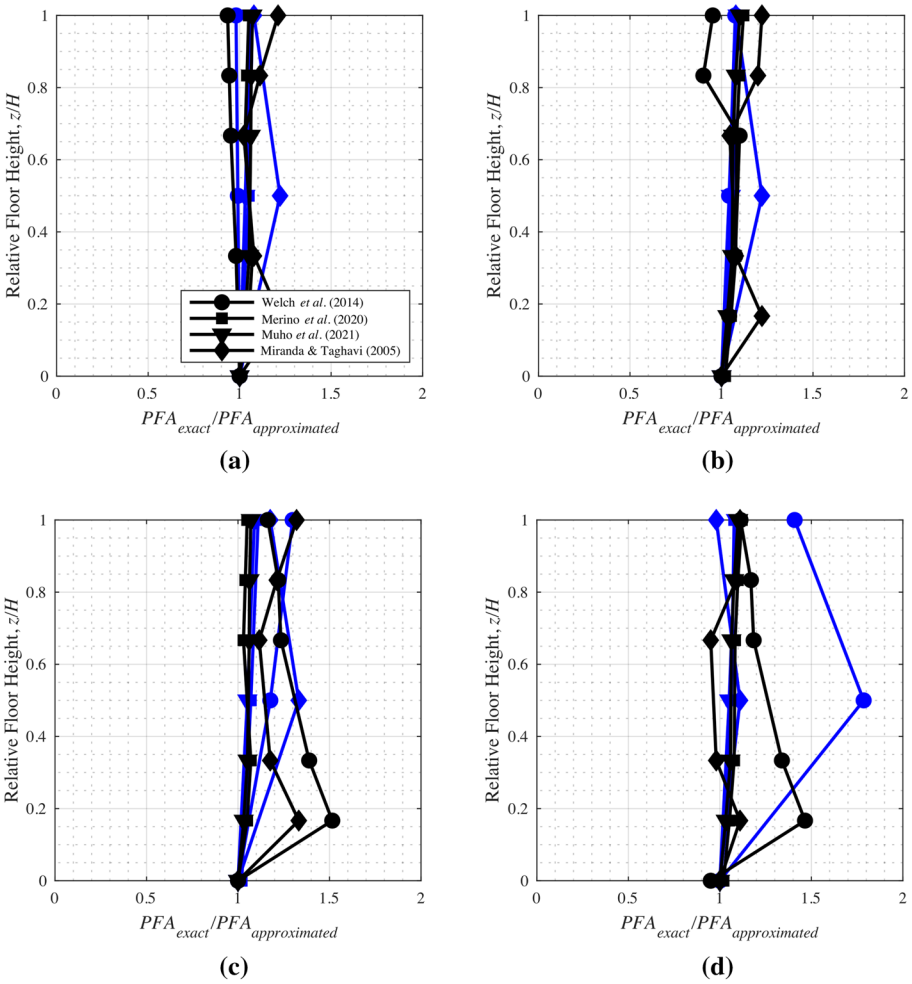


Fig. 9 Comparison of simplified methodologies to estimate peak floor acceleration demands in (blue) 2-storey and (black) 6-storey infilled RC frame buildings at **a** 30 years, **b** 50 years, **c** 475 years and **d** 975 years return period intensities

response is expected. The buildings whose results are demonstrated belong to a database of archetype models (O'Reilly and Nafeh 2021) and were fictitiously located in Napoli, Italy. The results were expressed in terms of the $PFA_{exact}/PFA_{approximate}$ ratio along the height of the structures, where PFA_{exact} is the resultant of extensive NLTHA where MSA was carried out at the four return periods highlighted, and $PFA_{approximate}$ corresponds to when simplified methods are used. The $PFA_{exact}/PFA_{approximate}$ is reported in Fig. 9 for the two case study structures. It highlights how the method described by (Welch et al. 2014b), particularly at higher return periods LSs such as 475 and 975 years, tends to underestimate the PFA demand. This may be due to the over-simplistic nature of the method, where a set of empirically-calibrated coefficients are used based on the structural typology of the system (i.e., moment-resisting frames, shear wall systems, braced systems). This calibration was not carried out specifically for infilled RC structures,

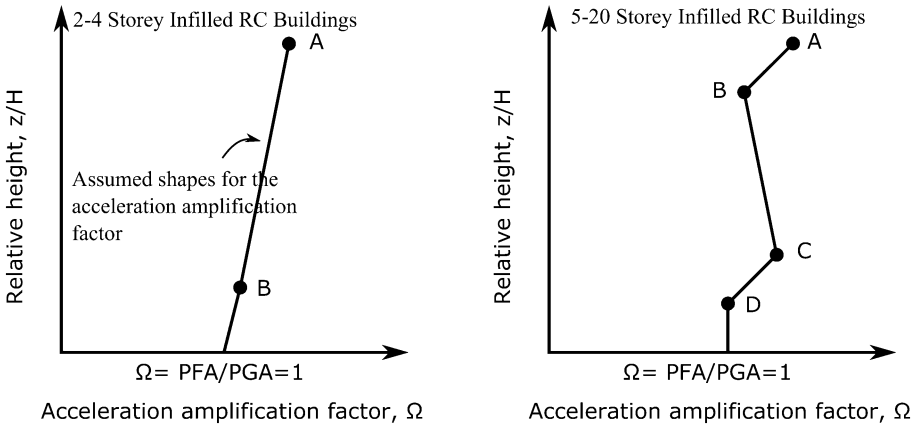


Fig. 10 Approximation of the acceleration amplification factor profiles for 2 to 4-storey (left) and 5–20 storey (right) infilled RC buildings (adapted from Muho et al. (Muho et al. 2021))

where the presence of infills and the formation of non-ductile mechanisms is expected; hence, the method is not expected to be applicable here. Moreover, the method of (Taghavi and Miranda 2005b) yielded consistently higher estimates across all return periods for both structures. Considering that conservativeness may appeal to practitioners when characterising structural demands, this may not be desirable in seismic loss estimation scenarios where overestimating the PFA demands leads to overestimating expected losses, particularly for non-structural components.

Figure 9 illustrates the robustness of the methods described in (Merino et al. 2020) and (Muho et al. 2021) in estimating PFA demands across all return period levels. As previously mentioned, (Merino et al. 2020) estimate PFA demands based on modal information easily retrieved from eigenvalue analysis along with spectral demands at the first period of the structure. On the other hand, the method of (Muho et al. 2021) relies on a relatively simple closed-form expression which accounts for the infill typology and other building characteristics. It can be seen from Fig. 9 that both methods performed relatively well even in the case where PFA demands were capped pre-maturely due to the formation of inelastic mechanisms at higher return periods (e.g., 975 years).

However, due to its practicality when compared to the method of (Merino et al. 2020) regarding the number of required parameters needed and its fair trade-off between accuracy and simplicity highlighted here, the method described by (Muho et al. 2021) was integrated within the *PB-Loss* framework to estimate PFA demands. As such the following procedure is advised to quantify PFA demands:

1. Select an approximate shape for the acceleration amplification factor, Ω based on the number of storeys as shown in Fig. 10;
2. The acceleration amplification factor $\Omega_{i,im}$, defined as the ratio between the PFA at floor i and the PGA for a given intensity, im can be estimated as:

$$\Omega_{i,im} = a_1 \theta_{i,im}^{a_2} T^{a_3} \left(\frac{E_2}{E_1}\right)^{a_4} t^{a_5} = \frac{PFA_{i,im}}{PGA_{im}} \tag{14}$$

where a_1, a_2, a_3, a_4, a_5 are calibrated parameters (Table 2) for each point on the expected shape of the acceleration amplification factor ; $\theta_{i,im}$ is the estimated PSD (in %) intensity *im* computed via Eq. (13); T is the fundamental period of the structure (in s); E_1 and E_2 are the horizontal and vertical moduli of elasticity of infill panels (in MPa), respectively; t is the thickness of the infill panels (in metres).

3.3.3 Residual peak storey drift

In addition to estimating economic losses based on peak response quantities such as PSD and PFA, permanent lateral deformations play a crucial role in overall performance (Mahin and Bertero 1981; Ruiz-Garcia and Miranda 2005c) and thus can have important economic consequences. Deformations are typically expressed in terms of the RPSD. When RPSD becomes larger, repairing damaged building components becomes impractical due to the permanent distortion in the structural skeleton. Several previous earthquakes (e.g., the 1985 Michoacán, Mexico and the 1995 Hyogo-ken Nambu, Japan) have witnessed buildings sustain residual drifts of approximately 1.75% with no collapse. However, due to the technical difficulties and large costs associated with the re-alignment of distorted buildings, government officials concurred on the need to demolish these buildings (Rosenblueth and Meli 1986; Kawashima 2000). To this end, the final component necessary for *PB-Loss* is the quantification of residual deformations. Ruiz-García and Miranda (2006a, 2006b) and (Ruiz-García and Chora 2015) propose coefficient-based simplified equations to estimate the RPSD quantities based on maximum inelastic displacements. Erochko et al. (2011) derived a simplified equation to estimate the expected residual drift based on analytical observations of steel moment-resisting frames and buckling-restrained braced frames. However, this expression may not be suitable for use when quantifying RPSD in infilled RC frame structures given the behaviour incompatibility. Therefore, the FEMA P-58 (FEMA 2012b) approximation was adopted to estimate the RPSD due to its independence of ground-motion characteristics and its simplistic implementation due to its empirical relationship to simple non-linear static metrics such as the storey drift at yield. The method assumes that the following criteria are satisfied: building response along each principal axis is uncoupled; the building is regular in plan and elevation (i.e., no significant discontinuities in lateral stiffness and strength); PSD does not exceed four times the drift at yield; storey drifts are less than 4% beyond which geometric non-linearity (i.e., P-Δ) effects become dominant. The approximation is given in Eq. (15).

$$\theta_{res,i,im} = 0 \qquad if\ \theta_{i,im} \leq \theta_y \tag{15}$$

Table 2 Empirical parameters for the quantification of the acceleration amplification factor of 2–20 storey infilled RC frame structures (adapted from (Muho et al. 2021))

Profile points	2–4 storeys					5–20 storeys				
	a_1	a_2	a_3	a_4	a_5	a_1	a_2	a_3	a_4	a_5
A	0.308	−0.460	0.055	−0.168	0.259	0.259	−0.438	−0.256	−0.270	0.196
B	0.645	−0.178	−0.148	−0.090	0.136	0.161	−0.463	−0.336	−0.291	0.145
C			–			0.708	−0.145	−0.206	−0.103	0.087
D			–			1.159	−0.027	−0.170	−0.048	0.076

$$\theta_{res,i,im} = 0.3\left(\theta_{i,im} - \theta_y\right) \qquad if\ \theta_y < \theta_{i,im} \le 4\theta_y$$

$$\theta_{res,i,im} = \left(\theta_{i,im} - 3\theta_y\right) \qquad if\ 4\theta_y < \theta_{i,im}$$

where $\theta_{res,i,im}$ is the estimated RPSD at a given *im* at floor *i*; $\theta_{i,im}$ is the estimated PSD at floor *i* (from Eq. (13); θ_y is the drift at yield determined using Eqs. (12) and (13). Naturally, the estimation of the RPSD must be carried out in both principal directions, where separate pushover analyses are carried out.

3.4 Collapse risk estimation

Table 1 listed the non-collapse intensities, *im* to be evaluated in *PB-Loss*. However, for the case of collapse, where the mean annual frequency of collapse (MAFC or λ_C) is unknown, the SAC/FEMA approach (Vamvatsikos 2013) is adopted. To estimate it, the approach adopted in *PB-Risk* is employed.

1. Fit a second-order approximation to the Sa_{avg} hazard curve, illustrated in Fig. 4a where $H(IM)$ denotes the mean annual rates of exceeding an *IM* value described by:

$$H(IM) = k_0 \exp\left[-k_2 ln^2(IM) - k_1 \ln(IM)\right] \tag{16}$$

where k_0, k_1 and k_2 are positive real numbers describing the coefficients of a second-order hazard fitting.

2. Calculate $\boldsymbol{\lambda_C}$ based on the closed-form intensity-based formulation proposed by Vamvatsikos (Vamvatsikos 2013)

$$\lambda_C = \sqrt{p} k_0^{1-p} \left[H\left(\widehat{Sa}_{avg,C}\right)\right]^p \exp\left[\frac{1}{2} p k_1^2 \beta_C^2\right] \tag{17}$$

$$p = \frac{1}{1 + 2k_2\beta_C^2} \tag{18}$$

where $\widehat{Sa}_{avg,C}$ and β_C are the median collapse intensity and associated dispersion identified from the response estimation tool described previously in Fig. 6.

3.5 Estimation of direct economic losses

The direct economic loss is taken as the sum of three mutually exclusive, collectively exhaustive events, conditioned on a ground-motion intensity *im*: non-collapse requiring repair, non-collapse requiring demolition and total replacement due to collapse. Subsequently, the EAL of the building can be evaluated by integrating the vulnerability curves with the site hazard curve given by Eq. (19).

$$EAL = \int E\left[L_T | IM = im\right] \left| \frac{dH(IM > im)}{dim} \right| dim \tag{19}$$

where the expected total economic loss term $E[L_T|IM = im]$ is the sum of the mutually exclusive, collectively exhaustive events, conditioned on a ground motion intensity IM = *im*, defined via:

$$E\left[L_T|IM=im\right] = E\left[L_T|NC, IM=im\right](1-P[C|IM=im]) + E\left[L_T|C\right]P[C|IM=im] \tag{20}$$

where $E\left[L_T|NC, IM=im\right]$ is the expected repair cost in the building given no collapse; $E\left[L_T|C\right]$ is the expected loss given collapse or simply the total replacement cost; $P[C|IM=im]$ is the collapse probability at an intensity $IM=im$ and it is typically a lognormal cumulative distribution expressed in terms of the median collapse intensity and the associated dispersion due to record-to-record variability and other sources (e.g., modelling uncertainties).

Moreover, Eq. (20) can be expanded further based on the recommendation of (Ramirez and Miranda 2009) to account for the probability of requiring demolition given the non-collapse of the building, $P[D|NC, IM=im]$ due to the excessive residual peak storey drifts (RPSD) as follows:

$$\begin{aligned} E\left[L_T|IM=im\right] =& E\left[L_T|NC\cap R, IM=im\right](1-P[D|NC, IM=im])(1-P[C|IM=im]) \\ &+ E\left[L_T|NC\cap D\right]P[D|NC, IM=im](1-P[C|IM=im]) + E\left[L_T|C\right]P[C|IM=im] \end{aligned} \tag{21}$$

where $E\left[L_T|NC\cap R, IM=im\right]$ is the expected repair at a given intensity im conditioned on non-collapse and the repairability of the building; $E\left[L_T|NC\cap D\right]$ is the expected loss given no collapse and the non-repairability of the building, which is likely equal to $E\left[L_T|C\right]$. The probability of demolition conditioned on non-collapse of the case study building at a given ground-motion level IM was computed herein as a function of the RPSD following the recommendations outlined in FEMA P-58 (FEMA 2012b) and (Ramirez and Miranda 2012). For this reason, a lognormally distributed probability function with a median of 1.5% and dispersion of 0.3 was considered.

EAL is nowadays considered a performance metric in loss-based applications (e.g. *Sismabonus* (Ministero delle Infrastrutture e dei Trasporti 2017; Cosenza et al. 2018)) which relates the expected monetary losses and the ground-shaking intensity through what is known as a *loss curve* (Fig. 12). A simplified procedure for constructing the different parts of this loss curve and subsequently estimating the EAL is presented in the following sub-sections.

3.5.1 Non-collapse: repairability

To estimate the repair cost ratio conditioned on non-collapse, the $E\left[L_T|NC\cap R, IM=im\right]$ term of Eq. (21) is evaluated. This defines the expected losses sustained following an earthquake event with intensity $IM=im$ that does not require demolition and repair actions can be carried out. The $E\left[L_T|NC\cap R, IM=im\right]$ term, calculated via storey-loss functions, denotes herein the percentage (i.e. of the total contribution of each PG to the total replacement cost at each $IM=im$. Therefore, it is more applicable by practitioners and engineers as it does not require knowing the total replacement cost of the building a priori. To estimate this, the generalised SLFs described here are used to find a quick and direct estimate of expected repair costs. As such, following the estimation of the PSD and PFA, previously described in Sects. 3.3.1 and 3.3.2, the user must:

1. Identify the most suitable SLF set from those available, or simply derive a set using the SLF generator proposed by Shahnazaryan et al. (Shahnazaryan et al. 2021);

2. For each separate PG, determine the expected loss ratio due to repair $E[L_T|NC \cap R, IM = im]_{PG,i}$ from SLFs using the relevant EDP and SLF pair at each intensity *im* and floor *I*;
3. Sum the contribution of each PG (in %) to the total repair costs at floor *i* as:

$$E\left[L_T|NC \cap R, IM = im\right]_i = \sum_{PG} E\left[L_T|NC \cap R, IM = im\right]_{PG,i} \tag{22}$$

4. Repeat the previous step for each floor *i*;
5. At each *im*, the total expected repair costs, expressed as a percentage of the total replacement cost, for the entire building can be derived as such:

$$E\left[L_T|NC \cap R, IM = im\right] = \sum_{i=1}^{N} E\left[L_T|NC, IM = im\right]_i \tag{23}$$

3.5.2 Non-collapse: demolition

As previously discussed, when a building possesses excessive permanent lateral deformation following an earthquake, repairability may not always prove feasible and thus demolition works may be required. In Eq. (21), this is expressed in terms of the term: $E\left[L_T|NC \cap D\right]P[D|NC, IM = im]$ where $E\left[L_T|NC \cap D\right]$ denotes the expected costs associated with demolition and $P[D|NC, IM = im]$ is the probability of requiring demolition. In most cases, the term $E\left[L_T|NC \cap D\right]$ is likely equal to the total replacement cost of the building.

The probability of demolition is calculated using the residual drift fragility proposed by (Ramirez and Miranda 2012). The probability that for a given value of RPSD, demolition would be required, is assumed to be lognormally distributed with a median of 1.5% and dispersion of 0.3. In *PB-Loss*, the maximum value of the estimated RPSD along the height (from Eq. (15) is used and a probability of demolition is obtained (as per Fig. 11).

$$P[D|NC, IM = im] = \Phi\left(\frac{\ln\left(RPSD/1.5\right)}{0.3}\right) \tag{24}$$

3.5.3 Collapse: total replacement

The total replacement of the structure due to collapse is defined by the term $E\left[L_T|C\right]P[C|IM]$ in Eq. (21), where $E\left[L_T|C\right]$ corresponds to the expected cost associated with the total replacement of a given structure (i.e., debris removal and complete replacement) and $P[C|IM = im]$ is the probability the building has collapsed. For example, a unit replacement cost such as €1192.27 per m^2 (Vecchio et al. 2018) may be adopted.

The collapse fragility function is expressed via a lognormal distribution where the median collapse intensity and associated dispersion, are retrieved from the response estimation tool described in Sect. 3.2 and shown in Fig. 6 to give:

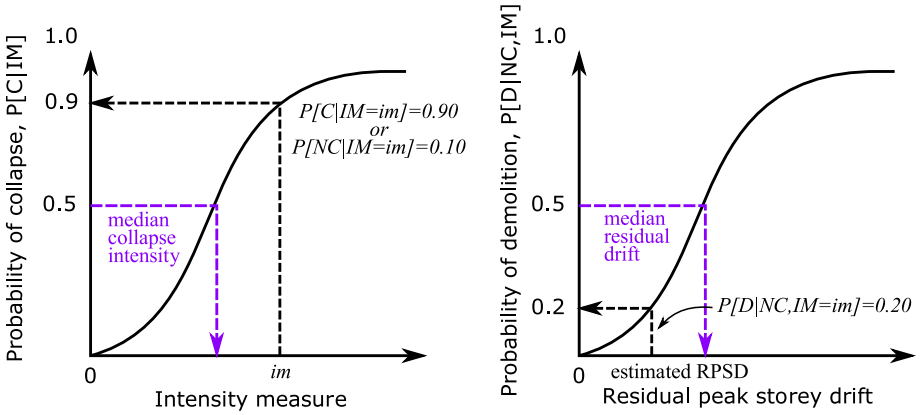


Fig. 11 Example illustration on the quantification of the probabilities of (left) collapse ($P[C|IM=im]$) and (right) demolition ($P[D|NC,IM=im]$)

$$P[C|IM = im] = \Phi\left(\frac{\ln\left(im \Big/ \widehat{Sa}_{avg,C}\right)}{\beta_C}\right) \tag{25}$$

Thus, for each identified *im*, a collapse probability can be evaluated as per Fig. 11.

3.5.4 Building the loss curve

The loss estimation of a case study building via *PB-Loss* concludes with the assembly of the loss curve, as illustrated in Fig. 12. This relates the total expected loss Eq. (21) to the intensity of ground-shaking sustained by a building at a particular site of interest. The EAL is then computed by integrating the loss curve via Eq. (19). To this end, the following steps are implemented:

1. For each intensity *im*, plot the total expected loss $E\left[L_T|IM = im\right]$ versus $H(IM)$;
2. An initial point is defined on the loss curve, namely the zero-loss (ZL) point, which represents the IM level where it is assumed that beyond this intensity, the losses are no longer non-negligible (i.e., $E\left[L_T|IM = im_{ZL}\right] = 0$). $H(im_{ZL})$ is assumed to be at a return period of 10 years, which is consistent with other simplified guidelines on risk assessment and loss quantification such as *Sismabonus* (Cosenza et al. 2018) and DEAL (Cardone et al. 2020), for example.
3. For collapse, the expected loss ratio is considered equal to be $E\left[L_T|C\right] = 1.0$ and the MAFC that describes its exceedance rate was previously quantified via Eq. (17).

3.5.5 Expected annual loss

To compute the EAL, the user must then integrate the area under the loss curve (i.e., $E[L_T|IM = im]$ vs $H(IM)$) as shown in Fig. 12. When a sufficient number of points have been established, the area can be evaluated using the trapezoidal rule given as:

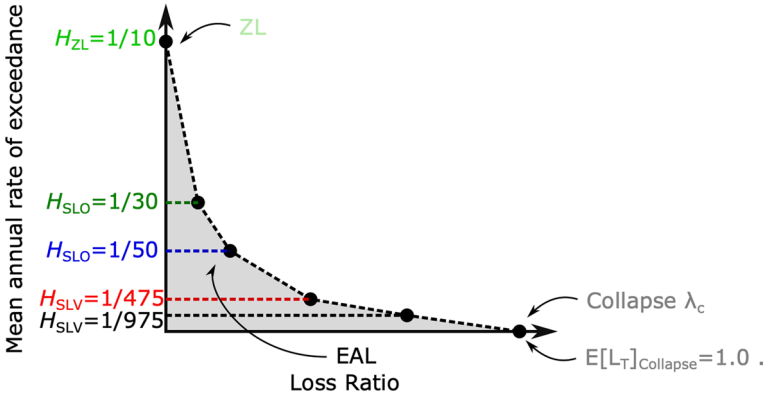


Fig. 12 Assembling the loss curve

$$EAL = \lambda_c E\left[L_T|C\right] + \sum_{i=2}^{n} \left|\lambda\left(im_i\right) - \lambda\left(im_{i-1}\right)\right| \left[\frac{\left[E\left[L_T|im_i\right] - E[L_T|im_{i-1}]\right]}{2}\right] \quad (26)$$

where $i=1$ and $i=n$ correspond to ZL and collapse, respectively; $\lambda(im)$ is the mean annual rate of exceeding an IM level or the reciprocal of the code-based return periods or LS. Furthermore, in applying *PB-Loss* herein, five non-collapse intensities were considered ($n=5$) but Eq. (26) is generalisable to consider additional intensities depending on the user's preferences regarding the degree of acceptable accuracy-computational effort trade-off.

4 Derivation of generalised storey loss functions for infilled RC buildings

This section discusses the development of generalised SLFs for simplified loss assessment of non-ductile infilled RC buildings illustrated in Fig. 13. The first step is the adequate characterisation of the analysed building. This requires properly identifying information related to the number of storeys, global dimensions, occupancy type, structural typology and other specific architectural features. When these are identified, a comprehensive consideration of the damageable component distribution is needed. To this end, a database of archetype buildings previously developed in (Nafeh and O'Reilly 2022) was utilised here. These infilled RC building archetypes were conceptualised and designed by simulating the design procedures used in various periods in Italy.

A thorough identification of the design space features with respect to key architectural characteristics was based on expert judgement following professional architectural consultation on current and past practices. The architectural considerations highlighted herein do not just reflect the archetype design space adopted but provide information on the building's structural and non-structural component inventory which are key elements in loss assessment and the current objective of this study. The geometric and architectural features selected to reflect the function and form of the regional design space includes, for example, narrow hallways and corridors in dwellings generally 150 cm wide; adjacent kitchens and bathrooms; plumbing fixtures installed based on optimised space allocation; adequate

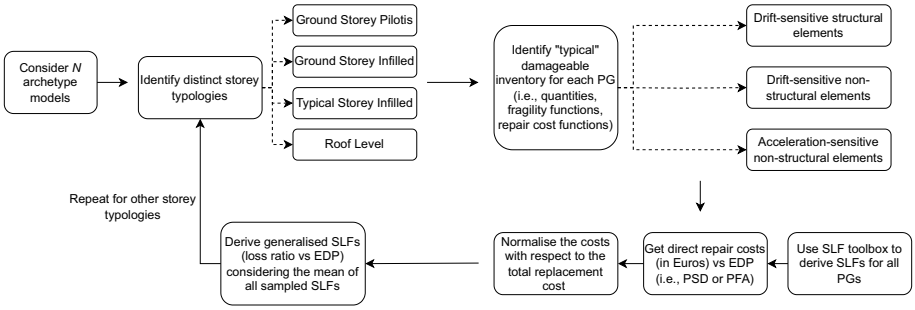
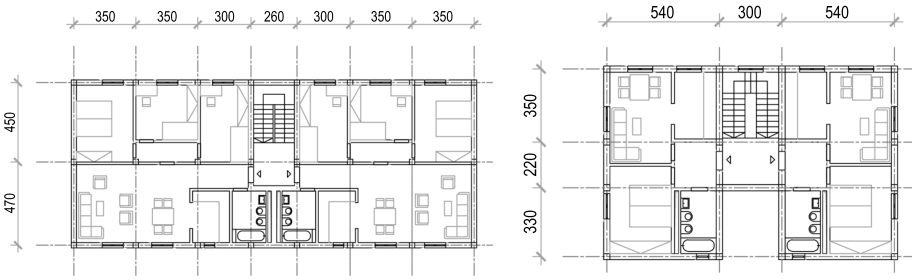


Fig. 13 Flowchart illustrating the necessary steps to derive generalised SLFs

separation of the day and night living spaces; windows with widths in multiples of 45 or 60 cm; staircase width not exceeding 3 m and landings depth not exceeding 1.3 m; double-leaf masonry infills for thermal and acoustic insulation and fire-retarding; 24 cm infill panels for perimeter walls of the façade; 30 cm infill panels for the separation of dwellings and encasing of the staircase; 80 mm single-leaf masonry infills or gypsum walls for internal partitioning and compartmentalisation of the living space. Once these characteristics were defined, an adequate identification of the non-structural components and anticipated building contents quantities was carried out for each archetype considered to identify the damageable inventory. An example of the plan layouts and architectural features is illustrated in Fig. 14.

Once the building characterisation is finalised, the damageable inventory defined in terms of fragility functions describing the various damage states of the components in addition to the expected repair costs is needed. The choices made during fragility and repair cost function identification must be as representative as possible of the regional construction and architectural context. The damageable inventory consists of structural and non-structural components and contents likely to sustain damage in the event of ground-shaking and contribute to overall economic losses. The considered damageable inventory related to each analysed archetype during the development of generalised SLFs and the respective quantities are available as an electronic supplement.

An aspect to consider when calibrating SLFs is distinguishing whether certain components will be affected by the PFA of the floor slab above or below the current storey.



(a) Archetype C (b) Archetype G

Fig. 14 Example of the archetype building layouts considered to derive storey loss functions

For example, ceiling fans are dependent on the PFA of the above floor, while home entertainment equipment will be sensitive to the PFA of the supporting floor. This aspect was accounted for in the SLF toolbox developed by (Shahnazaryan et al. 2021). Another important aspect is the orientation of damageable components, which is important for drift-sensitive components (i.e., infill panels, doors or windows) being damaged in mainly one direction, whereas acceleration-sensitive components were assumed orientation-independent. Therefore, the derived SLFs were obtained following assumptions on how the building components were oriented.

Once the inventory of damageable components has been identified, depending on the component type (i.e., structural or non-structural) and their EDP sensitivity (i.e., PSD or PFA), they are sorted into different PGs defined as drift-sensitive structural, drift-sensitive non-structural and acceleration-sensitive non-structural components. Relevant information on the fragility functions, damage states and associated repair costing for each component are provided in Appendix 1. The identified component inventory along with the fragility and consequences of various components are used as input for the SLF toolbox. The SLF toolbox then carries out Monte Carlo simulations. In each simulation run, damage and repair costs were sampled for every component within the PG. The cumulative cost for each component was then calculated to determine the total loss for the PG at a specific EDP. In the SLF toolbox, the procedure involves sampling damage states for each component across various EDP levels and a specified number of simulations. In essence, a random value ranging from 0 to 1 is generated to represent the likelihood of being in a damage state. This value is then utilised to assign a damage state to a component based on its fragility function. This process is reiterated for each component across the array of the damage states. Interested readers may refer to Shahnazaryan et al. (Shahnazaryan et al. 2021) for further detail on the implementation of the SLF toolbox.

Following the steps described, the SLFs were obtained based on the results of the 105 infilled RC archetype building models considered for this study. The SLFs are first presented in Fig. 15 in terms of the actual costs in Euros. The repair costs associated with each component of the damageable inventory (Tables 3 and 4) were adopted from the FEMA P-58 database with reasonable conversion to regional prices (Vecchio et al. 2018; Silva et al. 2020b). The expected repair costs for each storey typology considered and the relative contribution of each performance group are shown. Significant differences between the expected repair costs for the different storey typologies may be observed, which emphasises the need to distinguish storey typologies. This difference is mainly due to the damageable inventory and also the relative size of the storey's plan layout between buildings (i.e., ranging from 50–150 m^2 per dwelling). For example, as highlighted in Fig. 15b, for the case of ground-storey pilotis, the contribution of drift-sensitive structural components exceeds that of the other considered PGs. However, a lower contribution is observed for the remaining storey typologies due to the increased presence of non-structural components.

To facilitate the adoption of such SLFs, a more practical and simple approach is to use generalised SLFs. These are essentially the SLFs that have been derived for each archetype but are normalised directly to the total expected repair cost of all PGs. As such, the normalised expected repair costs associated with a particular PG or $E\left[\breve{\tilde{L}}|NC \cap R\right]_{PG,i}$ is the mean ratio of the total repair cost of that particular PG $RepC_{PG,i}$ by the total repair cost of the entire storey i (i.e., accounting for all PGs).

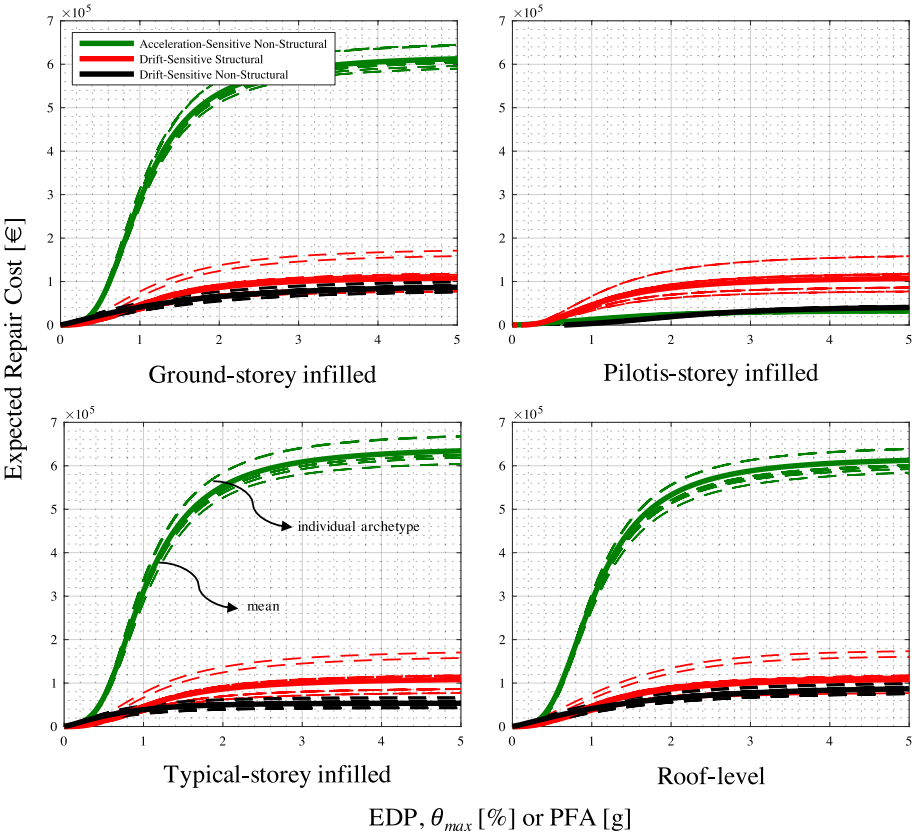


Fig. 15 Storey loss functions expressed in terms of the actual repair costs (in Euros) for each performance group (dotted lines: individual archetypes)

$$E\left[\breve{\tilde{L}}|NC \cap R\right]_{PG,i} = \frac{E\left[L_T|NC \cap R\right]_{PG,i}}{\sum_i E\left[L_T|NC \cap R\right]_{PG,i}} \tag{27}$$

As such, a clearer disaggregation of the repair costs associated with each PG can be observed and the estimation becomes independent of the total replacement value of the storey. This implies that should a representative normalising value be known for the building typology (or taxonomy class), estimates of repair costs could be quickly obtained by scaling the generalised SLF up by the expected repair cost value and integrated into engineering practice. This approach is seen as very advantageous for the *PB-Loss* methodology (in addition to others) as it paves the way for generalised SLFs to be developed for wide ranges of archetypes and proposed as reference SLFs for general applications. It is akin to how structural limit states are often assigned a repair cost value during other assessment methods like *Sismabonus*, except that SLFs provide a more refined and direct method of estimating loss as a function of the EDPs that generate losses in structures. Furthermore, SLFs may also be attributed other characteristics like energy efficiency when considering retrofitting options (Clemett et al. 2023), or also the repair class associated with different

damage states used to evaluate building recovery (Molina Hutt et al. 2022), but these topics are merely noted as potential future developments for SLFs.

The observed direct losses illustrated in Fig. 15 associated with each PG were normalised with respect to the total replacement cost corresponding to each archetype. The total replacement cost was calculated based on the total surface area of the building, where a unit replacement cost of €1192.27 per m^2 was utilised, as this was the value used for this typology during the L'Aquila reconstruction process (Vecchio et al. 2018). Generalised SLFs expressed in terms of a normalised loss ratio corresponding to the contribution of each PG were derived.

5 Comparison of *PB-Loss* with existing methods

An example application of the *PB-Loss* methodology is presented in Appendix 2 for a two-storey infilled RC building to demonstrate the case with which a loss assessment may be carried out. The following section then applies *PB-Loss* to many buildings to compare the proposed method with respect to other simplified methodologies available in the literature and national guidelines.

5.1 Existing loss assessment methodologies

A few notable proposals have been made among the different methods available to estimate economic losses in buildings. For example, DEAL (direct estimation of expected annual losses) is a simplified displacement-based approach developed by (Cardone et al. 2020) for pre-1970s existing RC buildings in Italy. DEAL evaluates the direct monetary losses via specific SLFs derived for pre-1970s existing Italian RC buildings after evaluating drift and acceleration demand through extensive NLTHA. The SLFs implemented in DEAL were previously derived from (Perrone et al. 2022) based on simple linear regression applied to results retrieved from PACT. It is important to note that these SLFs will conceptually differ from those proposed here since they represent a relationship between $E[L_T|IM = im]$ and EDP (i.e., it has already implemented Eqs. (20), (21), whereas the SLFs proposed here represent $E\left[L_T|NC \cap R, IM = im\right]$; hence, the collapse and repairability are handled with more precision here. The EAL values are then calculated using the closed-form expression outlined in Eq. (28), where the main assumptions are that the vulnerability and hazard curves can be simplified to a linear relationship, as proposed by (Sullivan 2016)

$$EAL = \lambda_{min} q_{min} + \frac{k_0}{Sa_{ZL}^k}\left[\frac{m}{1-k}\left(\sigma_{TL}^{1-k} - \sigma_{min}^{1-k}\right)\right] \tag{28}$$

where λ_{min} is the minimum annual frequency of exceedance taken as 10%; q_{min} is the minimum corresponding expected loss which depends mainly on the storey typology (i.e., infilled or pilotis); k_0 is the linear hazard fit coefficient; Sa_{ZL}^k is the zero-loss seismic intensity which represents the ground-shaking intensity below which only minor aesthetic damage is sustained, assumed to begin at a return period of 10 years; m is the slope of the adopted linear vulnerability function; $k = \frac{LOG\left(\frac{\lambda_{ULS}}{\lambda_{SLS}}\right)}{LOG\left(\frac{Sa(T*)_{ULS}}{Sa(T*)_{SLS}}\right)}$; σ_{TL}^{1-k} and σ_{min}^{1-k} denote the inten-

sity at which the normalised expected losses reach 100% of the replacement cost and the maximum normalised seismic intensity between the zero limit state and the spectral acceleration corresponding to the MAFE upper bound, respectively. λ_{SLS} and λ_{ULS} are the mean annual frequencies corresponding to the serviceability (i.e., a return period of 50 years) and ultimate limit states (i.e., a return period of 1000 years), respectively, and $Sa(T^*)_{SLS}$ and $Sa(T^*)_{ULS}$ are the spectral acceleration intensities at these return periods. For further details, the DEAL procedure is described in (Cardone et al. 2020) and the assumptions are illustrated in Fig. 17.

The Italian standards for the risk classification of buildings or *Sismabonus* introduced a set of guidelines for the seismic assessment of existing structures in Italy (Cosenza et al. 2018). These guidelines provide practitioners with relatively simple and fast tools. It classifies buildings quickly by characterising seismic risk via the "life-safety index" and the EAL, providing practitioners with simplified tools and incentivising the general public to perform seismic upgrades on existing buildings in the form of tax rebates of up to 110% of the costs. The approach is quite simple as it requires the analyst to conduct just a pushover analysis and eliminates the need for many of the steps involved in the PEER-PBEE loss estimation methodology described previously. The end result of the guidelines is an EAL estimate, that is classified within a letter-based system similar to that initially proposed by (Calvi et al. 2014). The structural performance is evaluated via non-linear static assessment procedures (e.g., the N2 method (Fajfar 2000)) at six different limit states. Once the seismic capacities and corresponding annual frequencies are computed, prescribed values of loss ratio associated with each limit state are used and expressed as %RepC. These are 0%, 7%, 15%, 50%, 80% and 100%, respectively, and do not consider the building occupancy type, size or other pertinent characteristics that a more detailed loss assessment would consider. This one-size-fits-all approach simplifies the assessment greatly but can lead to sensitive and sometimes subjective estimates of loss, directly impacting the assigned seismic risk class. These repair cost ratios are used to represent the λ-%RepC relationship and the EAL is evaluated as the area under the loss curve as:

$$EAL = \lambda(CLS)\%RepC(RLS) + \sum_{i=2}^{5} \left|\lambda\left(LS_i\right) - \lambda\left(LS_{i-1}\right)\right| \frac{\left[\%RepC\left(LS_i\right) - \%RepC\left(LS_{i-1}\right)\right]}{2} \tag{29}$$

Values of 0.35% and 8.215% represent the lower and upper bounds of the EAL estimates provided by the *Sismabonus* guidelines (Cosenza et al. 2018), which differ significantly from other values observed in other past studies for the same typology.

5.2 Comparative evaluation

The aforementioned simplified methodologies and the proposed *PB-Loss* approach are evaluated. These results are compared to the more rigorous component-based approach outlined in FEMA P-58 and are taken as the benchmark. To this end, a total of 70 infilled RC case study buildings for a site in L'Aquila, Italy. These case study buildings belong to a broader database of archetypes by (Nafeh and O'Reilly 2022) discussed previously.

Figure 18 illustrates the EAL values evaluated following the three simplified approaches compared to those obtained, and plotted against component-based assessment taken as

the benchmark. It is clear that the DEAL and *Sismabonus* significantly overestimate the EAL for all case study buildings. The main differences in the estimates provided by DEAL when compared to the EAL values obtained via extensive analysis results obtained from PACT arise from the simplifications made by DEAL. For example, the first assumption is related to the representation of hazard. DEAL assumes that the seismic hazard curve can be characterised with a first-order linear approximation in logspace whereas *PB-Loss* adopts a second-order fitting. The latter minimises the error whenever the curvature of the hazard function becomes significant (Vamvatsikos 2013). The second assumption relates to the simplified representation of economic losses. DEAL assumes that direct economic losses increase linearly with intensity (Sullivan 2016; Cardone et al. 2020). This leads to an overestimation of the losses, as observed in Fig. 18, especially when the simplification fits reasonably well at medium to high intensity, whose contribution to EAL is minimal, but fits quite poorly at low intensities, whose contribution to EAL is significant. For example, the main contributor to seismic losses at low to medium intensities is non-structural components where the trend between expected losses and the EDPs is not linear, seen in Figs. 15 and 16. On the other hand, *PB-Loss* adopts generalised SLFs derived based on the

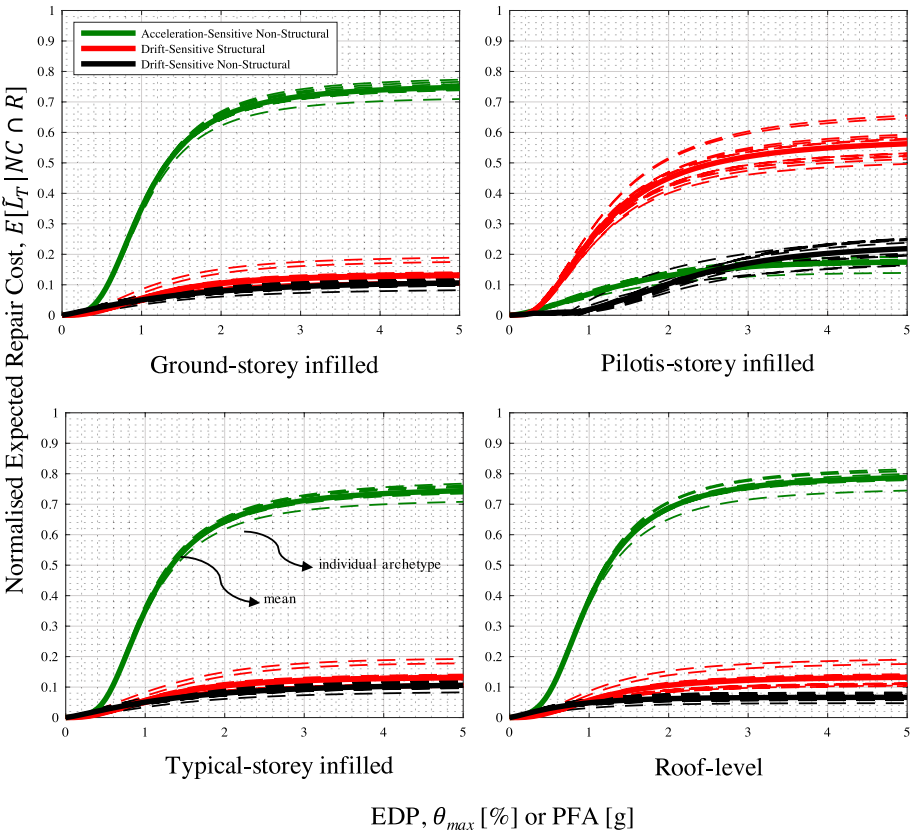


Fig. 16 Generic storey-loss functions relating the expected repair cost of a given performance group to the corresponding EDP

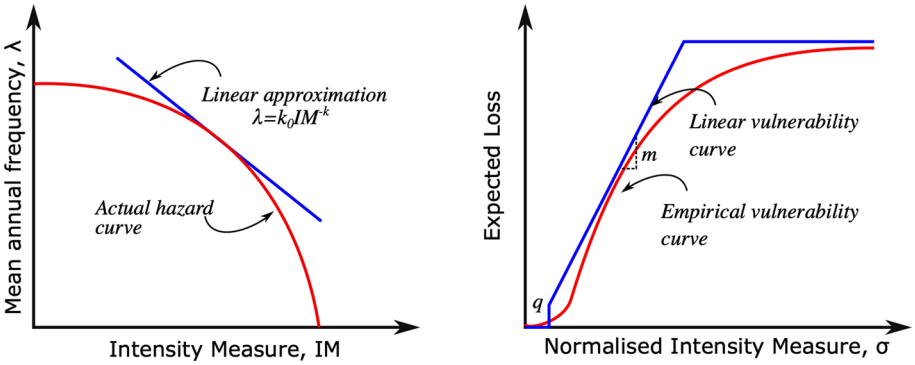


Fig. 17 Main assumptions of the DEAL approach proposed by (Cardone et al. 2020): a linear approximation of the hazard curve and the vulnerability curve

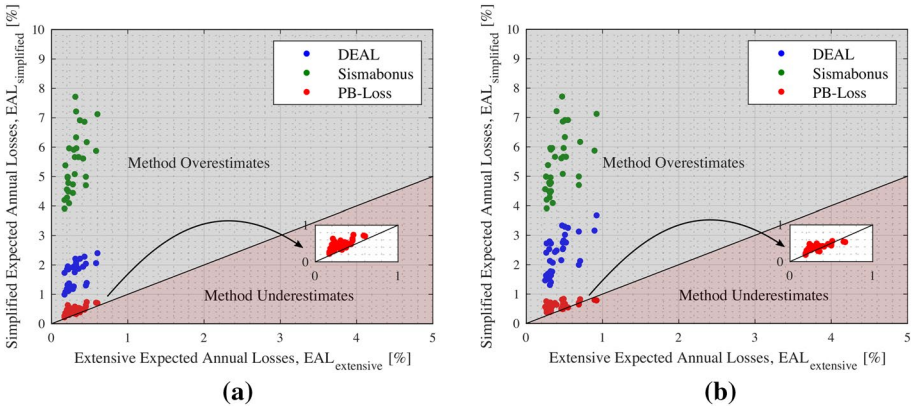


Fig. 18 Evaluation of *PB-Loss*, *Sismabonus* and DEAL, regarding their ability to estimate expected annual loss for (a) GLD and (b) SSD case study buildings

mean observed losses calibrated to several archetype-building models, meaning such errors were minimised, particularly at low-to-medium intensities (Fig. 17).

The main differences between the estimates obtained using *Sismabonus* and PACT invariably arise from the simplifications required to integrate the procedure outlined in *Sismabonus* with the existing code of practice in Italy. One of these is the expected loss ratios for each LS being fixed percentages of the replacement cost, regardless of building typology or occupancy. This aspect was investigated in (O'Reilly et al. 2018) by comparing the expected loss ratio at each LS from detailed analysis with the guidelines. It was shown that the expected loss ratios at each LS computed using detailed analysis were much lower than the fixed values specified in the guidelines, partly explaining the differences in the EAL values in Fig. 18. This was especially the case at the first few LSs which are weighted much more heavily during the EAL integration.

Moreover, it is evident from Fig. 18 that the proposed *PB-Loss* approach yielded relatively good estimates when compared to the extensive approach. This is due to the adaptability of the proposed SLFs in characterising the economic losses related to structural and non-structural damage. Based on these promising results regarding the accuracy of SLF-based loss assessment, integrating such simplified tools for the response estimation of structures in terms of demand parameters (i.e., PSD and PFA) should appeal to analysts. This integration could encourage a more demand-based estimation of losses at LSs or different levels of ground-shaking.

6 Summary and conclusions

Recent years have witnessed the evolution in seismic risk assessment from traditional objectives mainly related to building performance to other issues like economic loss and life safety. While loss assessment methods have been developed, the trade-off between simplicity and accuracy remains an open challenge for researchers in their attempts to provide engineers with simplified tools to use in practical applications. Evaluating the monetary losses sustained in seismic events, through metrics such as the expected annual losses (EAL), for example, is paramount for existing reinforced concrete (RC) structures with masonry infills due to their prevalence in the Mediterranean area.

In loss-based analysis, an accurate characterisation of structural performance is important, but non-linear time-history analyses (NLTHA) can be computationally expensive in terms of time and effort. Additionally, a rigorous component-based loss assessment approach is heavily dependent on assumptions made, which renders it equally laborious with regard to computational burden. While guidelines such as Sismabonus and DEAL attempt to mitigate such burdens, further scrutiny has shown that with respect to more exhaustive loss assessment methods, these simplified approaches possess some limitations and drawbacks that can be improved. This was shown seen here for non-ductile infilled RC buildings, which when assessed via current simplified approaches, were seen to give significantly different loss estimates from those obtained from more rigorous component-based analysis.

A novel *PB-Loss* methodology was proposed here to address these shortcomings and incorporate many facets currently overlooked in practical loss assessment. In summary, the *PB-Loss* encompasses the four main components for loss-assessment applications. First, hazard is characterised through probabilistic seismic hazard assessment and robust mathematical fitting. Second, the seismic vulnerability is identified through a response evaluation tool that empirically derives the seismic capacity of a given structure through a simple pushover analysis. Then, simplified assumptions and existing methodologies were integrated within *PB-Loss* to derive seismic demands such as the peak storey drifts (PSD), peak floor accelerations (PFA) and residual peak storey drift (RPSD) demands. Regarding the use of the response evaluation tool and the subsequent estimation of the drift demands, the integrated methods should be applied to regular buildings that are more likely to demonstrate a first-mode based shear-type response. As such, estimation errors may occur when contributions of higher-modes and torsional response (e.g. in high-rise or irregular

buildings) become more significant. Third, the SAC/FEMA approach is implemented to evaluate the collapse risk. Finally, generic storey-loss functions (SLFs) were derived to estimate the expected repair costs associated with different performance groups (PGs) and their corresponding EDPs. The *PB-Loss* method was outlined along with the tools and data needed for its implementation to infilled RC frame structures, with several examples provided to facilitate its widespread application. Some of the main outcomes of this study are:

- A comparative case study application on three different typologies (i.e., bare, pilotis and infilled RC) highlighted the robustness of the generalised SLF-based approach for evaluating economic losses when compared to the more rigorous component-based approach outlined in FEMA P-58.
- The proposed *PB-Loss* methodology was shown to evaluate the direct economic losses due to ground-shaking accurately and was validated within an illustrative case study application. The results highlighted the reliability and consistency of the proposed approach when compared to the results of the extensive analysis performed using FEMA P-58 on numerical models with hazard-consistent ground motions.
- Existing guidelines and methodologies for estimating economic losses such as *Sismabonus* and DEAL were also comparatively evaluated with respect to *PB-Loss*. Their results consistently overestimated the losses compared to the extensive component-based approach, whereas *PB-Loss* offers several improvements in this respect, such as consideration of PGs and their contributions from PSD and PFA sensitive components, RPSD, and collapse, rendering it a potential candidate for inclusion in the next generation of seismic loss estimation guidelines.

Appendix 1: Damageable Inventory

See Tables 3, 4, 5, 6, 7 and 8.

Table 3 Fragility function parameters and repair costs associated with the damage states exhibited by the considered structural elements

Component	Damage states (DSs)	EDP	Reference	Fragility Function Parameters		Costing Function Parameters	
				Median%	Dispersion	Mean Repair Cost €	Dispersion
Exterior beam-column joints with end-hooks	DS1 (light cracking)	Peak storey drift [%]	Cardone (2016)	0.75%	0.40	1284	0.45
	DS2 (concrete spalling)			1.25	0.40	2155	0.40
	DS3 (concrete crushing)			2.00	0.40	2895	0.42
Interior beam-column joints (weak column)	DS1 (light cracking)			0.65	0.40	1497	0.46
	DS2 (concrete spalling)			1.75	0.35	2574	0.41
	DS3 (concrete crushing)			3.00	0.30	4041	0.42
Non-ductile weak column	DS1 (light cracking)			0.95	0.30	882	0.47
	DS2 (concrete spalling)			1.25	0.40	1388	0.37
	DS3 (concrete crushing)			2.00	0.40	1747	0.41
Exterior masonry infills with windows	DS1 (light cracking)		Cardone and Perrone(2015)	0.10	0.50	62	0.22
	DS2 (extensive cracking)			0.30	0.50	117	0.44
	DS3 (corner crushing)			0.75	0.40	234	0.44
	DS4 (collapse)			1.75	0.35	234	0.52

Table 4 Fragility function parameters and repair costs associated with the damage states of the considered non-structural components

Component	Damage states (DSs)	EDP	Reference	Fragility function parameters		Costing function parameters	
				Median%	Dispersion	Mean Repair Cost €	Dispersion
Internal masonry infill partition (weak)	DS1 (light cracking)	Peak storey drift [%]	Cardone and Perrone (2015)	0.15	0.50	62	0.22
	DS2 (extensive cracking)			0.40	0.50	117	0.44
	DS3 (corner crushing)			1.00	0.40	234	0.44
	DS4 (collapse)			1.75	0.35	234	0.52
Stairs	DS1 (non-structural damage)		FEMA P-58–3 FEMA (2012b)	0.50	0.60	651	0.1
	DS2 (structural damage)			1.70	0.60	3441	
	DS3 (loss of live load capacity)			2.80	0.45	21,344	
Internal masonry infill partition (strong)	DS1 (operational)		Sassun et al. (2016)	0.18	0.52	35	
	DS2 (damage limitation)			0.46	0.54	62	
	DS3 (significant damage)			1.05	0.40	124	
	DS4 (near collapse)			1.88	0.38	124	
Gypsum infill partitions	DS1 (operational)			0.18	0.52	62	
	DS2 (damage limitation)			0.46	0.54	117	
	DS3 (significant damage)			1.05	0.40	234	
	DS4 (near collapse)			1.88	0.38	234	
Doors	DS1 (damaged)		O'Reilly et al. (2018)	1.88	0.38	754	
Windows	DS1 (damaged)			1.88	0.38	347	
Tables/Desks	DS1 (damaged)			1.88	0.38	191	
Chairs	DS1 (damaged)			1.88	0.38	24	
Independent pendant lighting (non-seismic)	DS1 (damaged)	Peak floor acceleration [g]	FEMA P-58 FEMA (2012b)	0.60 g	0.40	583	

Table 4 (continued)

Component	Damage states (DSs)	EDP	Reference	Fragility function parameters		Costing function parameters	
				Median%	Dispersion	Mean Repair Cost €	Dispersion
Home entertainment equipment	DS1 (falls, does not function)			0.80 g	0.40	1035	
Switchboards	DS1 (damaged, inoperative)			0.69 g	0.40	5569	
Lights	DS1 (disassembly of rod system at connections with horizontal light fixture, low cycle fatigue failure of the threaded road, pull-out of rods from ceiling assembly			1.00 g	0.40	583	
Water distribution piping system	DS1 (small leakage of joints)			0.55 g	0.40	307	
	DS2 (large leakage with major repair)			1.10 g	0.40	2302	
Heating distribution piping system	DS1 (small leakage of joints)			0.55 g	0.40	307	
	DS2 (large leakage with major repair)			1.10 g	0.40	2302	
Sanitary waste piping system	DS1 (small leakage of joints)			1.20 g	0.50	307	
	DS2 (large leakage with major repair)			2.40 g	0.50	2302	
Ceiling fans	DS1 (falls, non-functional)			1.40 g	0.60	250	
Distribution panels	DS1 (inoperative)			2.16 g	0.4	8770	
China and glassware	DS1 (object falls off shelf or shelf overturns and object breaks)			0.25 g	0.50	400	

Table 4 (continued)

Component	Damage states (DSs)	EDP	Reference	Fragility function parameters		Costing function parameters	
				Median%	Dispersion	Mean Repair Cost €	Dispersion
Bookshelves (unanchored)	DS1 (shelf overturns)			0.60 g	0.50	600	
Boiler unit	DS1 (non-functional)			0.60 g	0.50	3536	
Air conditioning unit	DS1 (non-functional)			0.60 g	0.50	450	

Table 5 Summary of the hazard assessment results and the identified *im* corresponding to Sa_{avg} and PGA at each NTC2018-based return period

Return Period, T_R (years)	Annual Rate of Exceedance, $H(im) = 1/T_R$		Intensity measure (*im*)	
			Average spectral acceleration, Sa_{avg} [g]	Peak ground acceleration, *PGA* [g]
30	0.033	34	0.106	0.045
50	0.020		0.148	0.069
475	0.0021		0.416	0.168
975	0.0010		0.539	0.213

Table 6 Summary of the performance points evaluated as part of *PB-Loss*

Return Period, T_R (years)	Average spectral acceleration, Sa_{avg} [g]	Ductility, μ		Mean annual frequency of exceedance (H and λ_c)
		X-direction	Y-direction	
10	0.076	–	–	0.10
30	0.106	0.24	0.26	0.033
50	0.148	0.34	0.36	0.021
475	0.416	0.95	1.02	0.0021
975	0.539	1.23	1.43	0.0010
Collapse	0.801	–	–	$\lambda_c = 6.85E\text{-}04$

Table 7 Summary of the simplified loss estimation corresponding to repair conditioned on non-collapse for each PG, $E[L_T|NC \cap R, IM = im]_{PG}$ in both principal directions of the case study building and the total repair cost per return period intensity

Return Period	Storey No	Drift-Sensitive Structural		Drift-Sensitive Non-Structural		Acceleration-Sensitive Non-Structural
		X-Direction	Y-Direction	X-Direction	Y-Direction	Uni-Directional
30	Ground	–	–	–	–	8.06E-05
	1st	1.43E-05	1.34E-05	0.0016	0.0022	0.0022
	2nd	4.35E-05	4.53E-05	0.0011	0.0042	0.0048
$E[L_T\|NC \cap R, IM = im_{30}]$	1.63%					
50	Ground	–	–	–	–	3.93E-04
	1st	2.12E-05	2.12E-05	0.0024	0.0015	0.0040
	2nd	6.16E-05	7.07E-05	0.0015	0.0011	0.0094
$E[L_T\|NC \cap R, IM = im_{50}]$	2.05%					
475	Ground	–	–	–	–	0.0085
	1st	7.73E-04	7.73E-04	0.0082	0.0091	0.1318
	2nd	6.16E-04	7.21E-04	0.0062	0.0067	0.1450
$E[L_T\|NC \cap R, IM = im_{475}]$	31.84%					
975	Ground	–	–	–	–	0.0204
	1st	0.0084	0.0050	0.0206	0.0167	0.2399
	2nd	0.0021	0.0015	0.0110	0.0098	0.3011
$E[L_T\|NC \cap R, IM = im_{975}]$	63.05%					

Table 8 Summary of the total loss ratio values per limit state intensity

Return Period, T_R (years)	Average spectral acceleration, Sa_{avg} [g]	Probability of demolition, P[D|RPSD]	Probability of collapse, P[C|IM]	Expected loss ratio at intensity $E[L_T\|IM = im]$ [%]
10	0.076	0.00	3.03E-11	0.0
30	0.106	0.00	9.67E-09	1.63
50	0.148	0.00	1.36E-06	2.05
475	0.416	1.25E-04	0.034	34.17
975	0.539	1.00	0.136	100
Collapse	0.801	1.00	1.00	100

Appendix 2: *PB-Loss* example application

Description of case study building

This section illustrates the application of the proposed *PB-Loss* methodology. To this end, a 2-storey non-ductile infilled RC building, taken from a database (O'Reilly and Nafeh 2021) of archetype numerical building models with taxonomy code GLD-D-2

was considered. The building was designed to resist gravity loads only with no consideration of ductile detailing and modern seismic provisions (i.e., pre-1970s). It was numerically modelled to capture the main inelastic mechanisms and potential failure modes. The model was developed in OpenSees (McKenna 2011) using a three-dimensional lumped plasticity approach. Figure 19. illustrates the plan layout and the numerical model of the building considered for this case study application. Beam and column members were modelled as elastic beam-column elements with cracked section properties and zero-length elements located at a finite plastic hinge length (Domenico et al. 2021; O'Reilly and Sullivan 2019). Beam-column joints were modelled by adopting a scissor-type modelling approach. Adequate considerations for exterior and interior joints were adopted, reflecting the poor detailing and use of smooth rebars with end-hooks during that period (Risi et al. 2017; Risi and Verderame 2017). Masonry infill panels were modelled using the equivalent strut approach (Crisafulli et al. 2000), and the difference in infill strength (i.e., weak, medium and strong) used was considered following the characterization of Hak et al. (Hak et al. 2012). Further details on the adopted numerical modelling techniques and design considerations are provided in Nafeh and O'Reilly (Nafeh and O'Reilly 2022).

Seismic hazard assessment and intensity measure identification

To identify the seismic hazard, the building was assumed to be located in Napoli, Italy. Probabilistic seismic hazard analysis was carried out using the OpenQuake engine to obtain the mean hazard curve in terms of Sa_{avg} and PGA as the IMs; For the case of Sa_{avg}, this was defined between periods of 0.2 T^* and 2 T^*, where T^* is the geometric mean of the first-mode periods in both principal directions (i.e., $T_{1,x}=0.19$ s and $T_{1,y}=0.21$ s). The ESHM13 hazard model (Woessner et al. 2015) combined with the site characteristics of Mori et al. (Mori et al. 2020) was used. Once the mean hazard curves at the site of interest were obtained, the *im* values of each code-defined return period were identified and reported in Table 5. Subsequently, Eq. (16) was fitted to the Sa_{avg} hazard curve via least-squares regression outlined by Shahnazaryan and O'Reilly (Shahnazaryan and O'Reilly 2023) to obtain $k_0=2.09\text{e-}04$, $k_1=3.20$ and $k_2=0.43$, where an R^2 value of 0.91 was noted.

Seismic vulnerability assessment: non-collapse and collapse capacities

Using the numerical model, a modal analysis was carried out to determine the first-mode shape ordinates, $\Phi_{1,x}=\{0, 0.65, 1.00\}$ and $\Phi_{1,y}=\{0, 0.69, 1.00\}$ were determined for the X and Y directions respectively. A first-mode transformation factor, Γ_x and Γ_y, of 1.25 and 1.28 were determined for the X and Y directions, respectively. These are necessary to compute the equivalent single degree of freedom (SDOF) properties as described in Sect. 3.2. Furthermore, non-linear static pushover analyses were conducted for the case study building in the two principal directions. To this end, a displacement-controlled inverse triangular lateral load pattern was used, whose results are illustrated in Fig. 20. Also illustrated are the multi-linearisation and the SDOF backbone capacity required for the response evaluation tool (Nafeh and O'Reilly 2022). The multi-linearisation was performed graphically to the onset and end of each response branch highlighted in Fig. 20, namely the elastic, hardening, softening and the residual plateau branches. Multiple verification criteria are implemented within the tool (as illustrated previously in Fig. 5). For example, the initial stiffness of the system via the fitting (i.e. the definition of the yield point) must match approximately

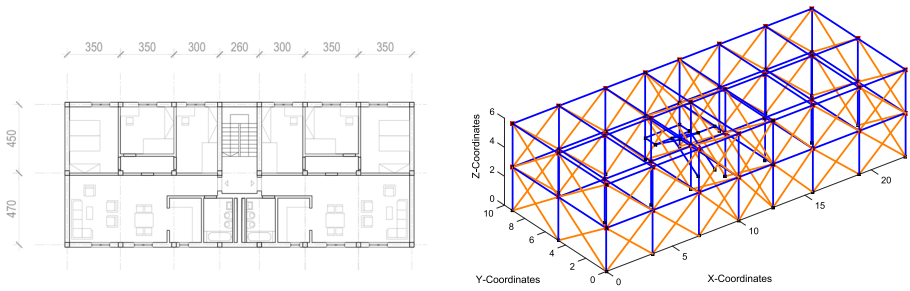


Fig. 19 **a** Architectural plan layout and **b** numerical model of the two-storey infilled RC building GLD-D-2

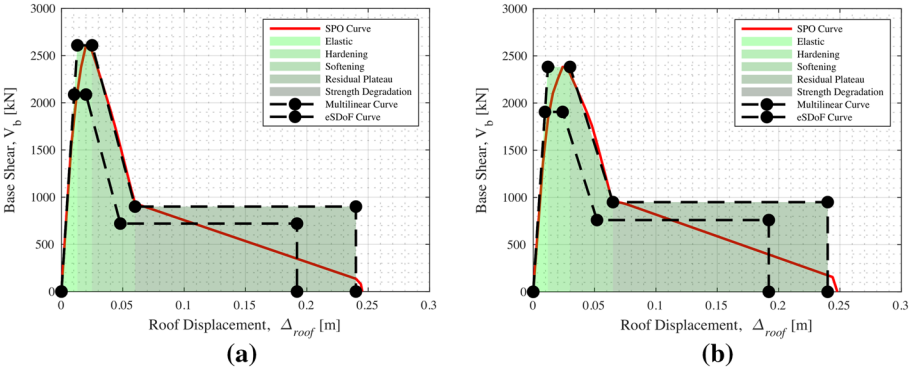


Fig. 20 Multi-linearisation of the MDOF pushover curve following SPO analyses carried out in both principal directions and the equivalent SDOF backbone capacity used in the response estimation tool

80% that of the actual SPO curve, consequently ensuring a period match between the SDOF and the actual multi-degree of freedom system (MDOF).

The seismic demand-intensity model was calculated for the structure in both directions using the ρ–μ–T functions previously developed by Nafeh and O'Reilly (Nafeh and O'Reilly 2022) and implemented in the response evaluation tool. As such, the dynamic capacities were first derived for the SDOF and then converted using Eqs. (9) and (10). As such, the response of the MDOF system is consequently characterised in terms of the Sa_{avg} and the maximum roof displacement. These results are demonstrated in Fig. 21. Additionally, the *im* levels previously reported in Table 5, were identified on the capacity curves of Fig. 5 along with the median collapse intensity and the associated dispersion.

Seismic demand estimation

Following the characterisation of the seismic vulnerability, the ductility of the MDOF at each intensity measure level, μ_{im} were calculated and are reported in Table 6. The resulting peak storey drift (PSD) profiles were derived as per Eqs. (12) to (13) whereas

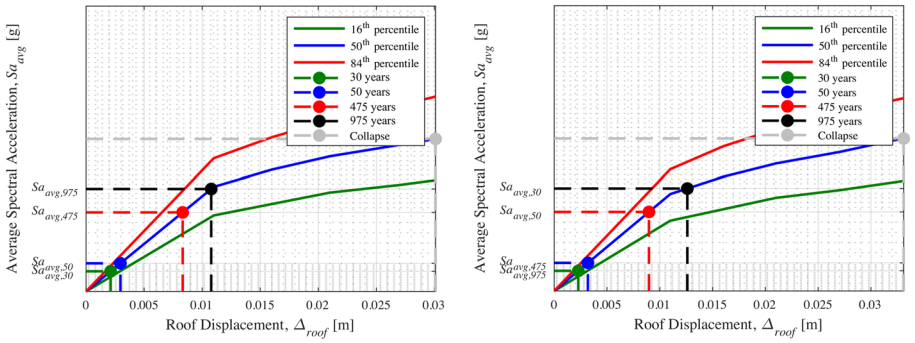


Fig. 21 Dynamic capacity curves for collapse and non-collapse expressed in terms of Sa_{avg} and the roof displacement following the application of ρ-μ-T relationships (Nafeh and O'Reilly 2022) integrated in the response estimation tool

the peak floor acceleration (PFA) profiles were approximated based on the approach outlined in Muho et al. (Muho et al. 2021) described in Sect. 3.3.2. For PFA demands, an "A-B" approximate shape was selected for the acceleration amplification factor as per Fig. 10. Given the diverse infill typologies (i.e., weak, medium and strong) present in the three-storey building, weighted average values were assigned to the horizontal and vertical infill moduli of elasticity and thickness, based on the total number of infill panels when using Eq. (14). To estimate the residual peak storey drifts (RPSD) per Eq. (15), the drift at yield, θ_y, was calculated using Eq. (12) to and is approximately 0.16%. During the application of the FEMA P-58 approach for the estimation of RPSD quantities, it was observed that for SLO and SLD, no RPSD was expected since the peak storey drift demands were smaller than θ_y. The demand profiles corresponding for PFA, PSD and RPSD are illustrated in Fig. 22.

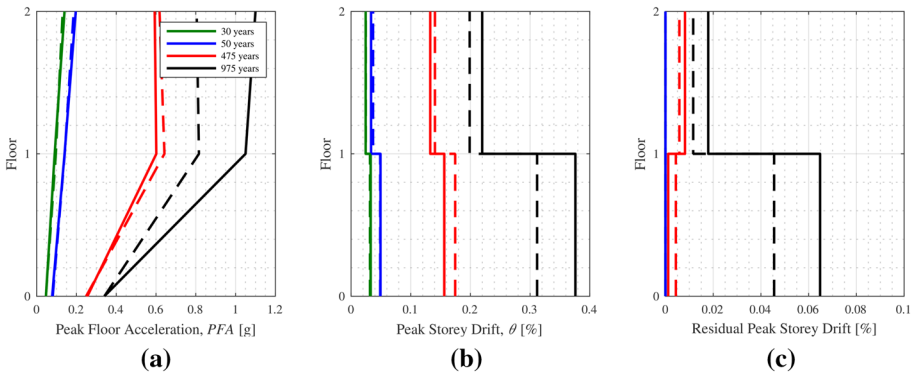


Fig. 22 Demand profiles for peak floor accelerations, peak storey drifts and the residual peak storey drifts for the X-direction (solid lines) and Y-direction (dashed lines)

Seismic risk evaluation: non-collapse and collapse risk

The annual rates of exceedance at the non-collapse intensities were determined from the hazard curve $H(IM)$ as the reciprocal of the code-based return periods, previously reported in the second column of Table 5.

The seismic collapse risk or the mean annual frequency of collapse (MAFC or λ_c) was determined from Eqs. (17) and (18). This requires the hazard coefficients (previously reported in Sect. 8.2) and the median collapse intensity and associated dispersion. The median collapse intensities and their associated uncertainties, retrieved from the response estimation tool, and annotated in Fig. 21 were employed. Collapse occurs simultaneously regardless of the independent state of the structure in both directions; hence, the more critical of the collapse fragility in both directions was utilised to calculate the MAFC. The annual rates of exceedance for both collapse and non-collapse cases are summarised in the last column Table 6.

Seismic loss evaluation

Knowing the PSD and PFA demand profiles illustrated in Fig. 22, the expected loss ratio corresponding to the repair of each PG and conditioned on non-collapse or $E[L_T|NC \cap R, IM = im]$ from Sect. 3.5.1 can be estimated using the derived generalised storey-loss functions (SLFs), presented previously in Fig. 16. As such, the SLFs of Fig. 16a was used for the infilled ground storey, (c) for the typical infilled storey and (d) for the roof level. Once the loss ratios were determined for each performance group (PG) at each storey via interpolation, the total loss ratio on each level at each intensity for the entire case study building, which are reported in Table 7, can be calculated.

To estimate losses associated with demolition due to excessive non-repairable residual drifts and the total replacement of a building due to collapse, the probabilities of demolition and collapse must be retrieved, respectively. To do so, the recommendations previously stated in Sects. 3.5.2 and 3.5.3 were considered. To this end, the collapse probability was identified as a lognormal distribution with a median collapse intensity $\widehat{Sa}_{avg,C}$ 0.801 g and an associated dispersion of 0.38. The demolition probability was derived based on a lognormally distributed function with a median RPSD of 1.5% and a dispersion of 0.3. These are both shown in Fig. 21. For each return period-based

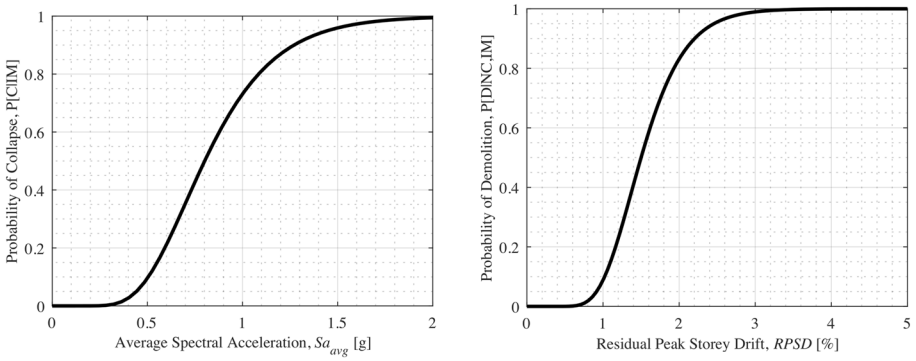


Fig. 23 The collapse (left) and demolition (right) fragility functions used for the case study building

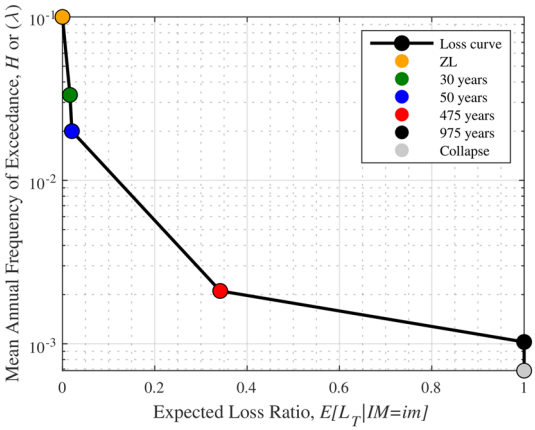


Fig. 24 Loss curve expressing the expected loss ratios in terms against the mean annual rate of exceedances obtained following the *PB-Loss* approach for the case study building

intensity listed in Table 6; the probability of demolition or collapse (Fig. 23) was computed and are reported in the third and fourth columns of Table 8.

Combining the information gathered in Table 7 and the probabilities of demolition and collapse, Eq. (21) can be applied to evaluate the expected loss ratio at each intensity, $E[L_T|IM = im]$, reported in the 3rd and 4th columns of Table 8.

With these values of annual rate of exceedance and the expected loss ratio at each intensity reported in Table 6 the loss curve can be constructed, and is shown in Fig. 24. The expected annual loss (EAL) is determined as the area under the loss curve using Eq. (26), which for this case study gave a value of 1.88%.

Author contributions Both authors contributed to the study conception and design. Material preparation, data collection and analysis were performed by AMBN. The first draft of the manuscript was written by AMBN and GJO commented and edited on subsequent versions of the manuscript. Both authors read and approved the final manuscript.

Funding The work presented in this paper has been developed within the framework of the projects "Dipartimenti di Eccellenza", funded by the Italian Ministry of Education, University and Research at IUSS Pavia.

Availability of data and material The building models used as part of this study are freely available on Github at: https://github.com/gerardjoreilly/Infilled-RC-Building-Database, The generalised storey-loss functions data developed primarily in this study are freely available on Github at: https://github.com/gerardjoreilly/Infilled-RC-Building-Database,

Code availability The code used for response estimation is freely available on Github at: https://github.com/gerardjoreilly/Infilled-RC-Building-Response-Estimation.

Declarations

Conflict of interest The authors have no conflicts of interest to declare that are relevant to the content of this article.

References

Akkar S, Yazgan U, Gülkan P (2005) Drift estimates in frame buildings subjected to near-fault ground motions. J Struct Eng 131(7):1014–1024. https://doi.org/10.1061/(ASCE)0733-9445(2005)131:7(1014)

Alirezaei M, Noori M, Tatari O, Mackie KR, Elgamal A (2016) BIM-based damage estimation of buildings under earthquake loading condition. Procedia Eng 145:1051–1058. https://doi.org/10.1016/j.proeng.2016.04.136

Almufti I, Willford M. (2013) REDi™ Rating system: resilience-based earthquake design initiative for the next generation of building. DOI: https://doi.org/10.13140/RG.2.2.20267.75043

Alonso-Rodríguez A, Miranda E (2016) Dynamic behavior of buildings with non-uniform stiffness along their height assessed through coupled flexural and shear beams. Bull Earthq Eng 14(12):3463–3483. https://doi.org/10.1007/s10518-016-0009-2

ATC 58–1 (2011) Guidelines for seismic performance assessment of buildings: vol 1—methodology. Redwood City

Baltzopoulos G, Baraschino R, Iervolino I, Vamvatsikos D (2017) SPO2FRAG: software for seismic fragility assessment based on static pushover. Bull Earthq Eng 15(10):4399–4425. https://doi.org/10.1007/s10518-017-0145-3

Blasi G, Perrone D, Aiello MA (2018) Fragility functions and floor spectra of RC masonry infilled frames: influence of mechanical properties of masonry infills. Bull Earthq Eng 16(12):6105–6130. https://doi.org/10.1007/s10518-018-0435-4

Calvi GM, Sullivan TJ, Welch DP (2014) A seismic performance classification framework to provide increased seismic resilience. In: A. Ansal (ed.), editor. Perspectives on European Earthquake Engineering and Seismology. DOI: https://doi.org/10.1007/978-3-319-07118-3_11.

Cardone D (2016) Fragility curves and loss functions for RC structural components with smooth rebars. Earthq Struct 10(5):1181–1212. https://doi.org/10.12989/eas.2016.10.5.1181

Cardone D, Perrone G (2015) Developing fragility curves and loss functions for masonry infill walls. Earthq Struct 9(1):257–279. https://doi.org/10.12989/eas.2015.9.1.257

Cardone D, Perrone G, Flora A (2020) Displacement-based simplified seismic loss assessment of pre-70S RC buildings. J Earthq Eng 24(sup1):82–113. https://doi.org/10.1080/13632469.2020.1716890

Clemett N, Carofilis Gallo WW, Gabbianelli G, O'Reilly GJ, Monteiro R (2023) optimal combined seismic and energy efficiency retrofitting for existing buildings in Italy. J Struct Eng. https://doi.org/10.1061/(ASCE)ST.1943-541X.0003500

CNR (2014) Istruzioni per la Valutazione Affidabilistica della Sicurezza Sismica di Edifici Esistenti

Cornell CA, Krawinkler H (2000) Progress and challenges in seismic performance assessment. PEER Center News 3(2):1–4

Cornell CA, Jalayer F, Hamburger RO, Foutch DA (2002) Probabilistic basis for 2000 SAC federal emergency management agency steel moment frame guidelines. J Struct Eng 128(4):526–533. https://doi.org/10.1061/(ASCE)0733-9445(2002)128:4(526)

Cosenza E, Del Vecchio C, Di Ludovico M, Dolce M, Moroni C, Prota A et al (2018) The Italian guidelines for seismic risk classification of constructions: technical principles and validation. Bull Earthq Eng 16(12):5905–5935. https://doi.org/10.1007/s10518-018-0431-8

Crisafulli FJ, Carr AJ, Park R (2000) Analytical modelling of infilled frame structures—a general review. Bull N Z Soc Earthq Eng 33(1):30–47. https://doi.org/10.5459/bnzsee.33.1.30-47

De Risi MT, Verderame GM (2017) Experimental assessment and numerical modelling of exterior non-conforming beam-column joints with plain bars. Eng Struct 150:115–134. https://doi.org/10.1016/j.engstruct.2017.07.039

De Risi MT, Ricci P, Verderame GM (2017) Modelling exterior unreinforced beam-column joints in seismic analysis of non-ductile RC frames. Earthq Eng Struct Dyn 46(6):899–923. https://doi.org/10.1002/eqe.2835

Del Vecchio C, Di Ludovico M, Pampanin S, Prota A (2018) Repair costs of existing RC buildings damaged by the l'aquila earthquake and comparison with FEMA P-58 predictions. Earthq Spectra 34(1):237–263. https://doi.org/10.1193/122916EQS257M

Di Domenico M, Ricci P, Verderame GM (2021) Empirical calibration of hysteretic parameters for modelling the seismic response of reinforced concrete columns with plain bars. Eng Struct 237:112120. https://doi.org/10.1016/j.engstruct.2021.112120

Eads L, Miranda E, Lignos DG (2015) Average spectral acceleration as an intensity measure for collapse risk assessment. Earthq Eng Struct Dynam 44(12):2057–2073. https://doi.org/10.1002/eqe.2575

Erochko J, Christopoulos C, Tremblay R, Choi H (2011) Residual drift response of SMRFs and BRB frames in steel buildings designed according to ASCE 7–05. J Struct Eng 137(5):589–599. https://doi.org/10.1061/(ASCE)ST.1943-541X.0000296

Eroğlu T, Akkar S (2011) Lateral stiffness estimation in frames and its implementation to continuum models for linear and nonlinear static analysis. Bull Earthq Eng 9(4):1097–1114. https://doi.org/10.1007/s10518-010-9229-z

European Standard (2004) Eurocode 8: design of structures for earthquake resistance—Part 1: general rules, seismic actions and rules for buildings. European Committee for Standardization
Fajfar P (2000) A nonlinear analysis method for performance-based seismic design. Earthq Spectra 16(3):573–592. https://doi.org/10.1193/1.1586128
FEMA (2012) Seismic performance assessment of buildings volume 1—methodology. FEMA P-58–1. Federal Emergency Management Agency **1**(August): 278
FEMA (2012) Seismic performance assessment of buildings: volume 2—Implementation guide. Fema: 365
FEMA (2012) FEMA P58–1. Seismic performance assessment of buildings: Volume 1—Methodology (P-58–1) vol 1 Washington, DC
Guerrini G, Graziotti F, Penna A, Magenes G (2017) Improved evaluation of inelastic displacement demands for short-period masonry structures. Earthq Eng Struct Dyn 46(9):1411–1430. https://doi.org/10.1002/eqe.2862
Hak S, Morandi P, Magenes G, Sullivan TJ (2012) Damage control for clay masonry infills in the design of RC frame structures. J Earthq Eng 16(SUPPL. 1):1–35. https://doi.org/10.1080/13632469.2012.670575
Haselton-Baker Risk Group (2020) Seismic Performance Prediction Program SP3
Heidebrecht A, Stafford SB (1973) Approximate analysis of tall wall-frame structures. J Struct Div 99:199–221
Kawashima K (2000) Seismic design and retrofit of bridges. In: The 12th World Conference on Earthquake Engineering, Auckland
Khaloo AR, Khosravi H (2008) Multi-mode response of shear and flexural buildings to pulse-type ground motions in near-field earthquakes. J Earthq Eng 12(4):616–630. https://doi.org/10.1080/13632460701513132
Lai X, He Z, Wu Y (2021) Elastic inter-story drift seismic demand estimate of super high-rise buildings using coupled flexural-shear model with mass and stiffness non-uniformities. Eng Struct 226:111378. https://doi.org/10.1016/j.engstruct.2020.111378
Lin T, Haselton CB, Baker JW (2013) Conditional spectrum-based ground motion selection. Part I: hazard consistency for risk-based assessments. Earthq Eng Struct Dyn 42(12):1847–1865. https://doi.org/10.1002/eqe.2301
Mahin SA, Bertero VV (1981) An evaluation of inelastic seismic design spectra. J Struct Div 107(9):1777–1795. https://doi.org/10.1061/JSDEAG.0005782
McKenna F (2011) OpenSees: a framework for earthquake engineering simulation. Comput Sci Eng 13(4):58–66. https://doi.org/10.1109/MCSE.2011.66
Merino RJ, Perrone D, Filiatrault A (2020) Consistent floor response spectra for performance-based seismic design of nonstructural elements. Earthq Eng Struct Dyn 49(3):261–284. https://doi.org/10.1002/eqe.3236
Ministero delle Infrastrutture e dei Trasporti (2017) Sismabonus: Decreto Ministeriale 58/2017
Miranda E, Akkar SD (2006) Generalized interstory drift spectrum. J Struct Eng 132(6):840–852. https://doi.org/10.1061/(ASCE)0733-9445(2006)132:6(840)
Miranda E, Reyes CJ (2002) Approximate lateral drift demands in multistory buildings with nonuniform Stiffness. J Struct Eng 128(7):840–849. https://doi.org/10.1061/(ASCE)0733-9445(2002)128:7(840)
Miranda E, Taghavi S (2005a) Approximate floor acceleration demands in multistory buildings. I: formulation. J Struct Eng 131(2):203–211. https://doi.org/10.1061/(ASCE)0733-9445(2005)131:2(203)
Molina Hutt C, Vahanvaty T, Kourehpaz P (2022) An analytical framework to assess earthquake-induced downtime and model recovery of buildings. Earthq Spectra 38(2):1283–1320. https://doi.org/10.1177/87552930211060856
Mori F, Mendicelli A, Moscatelli M, Romagnoli G, Peronace E, Naso G (2020) A new Vs30 map for Italy based on the seismic microzonation dataset. Eng Geol 275:105745. https://doi.org/10.1016/j.enggeo.2020.105745
Muho EV, Pian C, Qian J, Shadabfar M, Beskos DE (2021) Deformation-dependent peak floor acceleration for the performance-based design of nonstructural elements attached to R/C structures. Earthq Spectra 37(2):1035–1055. https://doi.org/10.1177/8755293020988015
Nafeh AMB, O'Reilly GJ (2022) Unbiased simplified seismic fragility estimation of non-ductile infilled RC structures. Soil Dyn Earthq Eng 157:107253. https://doi.org/10.1016/j.soildyn.2022.107253
Nafeh AMB, O'Reilly GJ (2023) Simplified pushover-based seismic risk assessment methodology for existing infilled frame structures. Bull Earthq Eng. https://doi.org/10.1007/s10518-022-01600-y

Nafeh AMB, O'Reilly GJ, Monteiro R (2020) Simplified seismic assessment of infilled RC frame structures. Bull Earthq Eng 18(4):1579–1611. https://doi.org/10.1007/s10518-019-00758-2
Neam AS, Taghikhany T (2016) Prediction equations for generalized interstory drift spectrum considering near-fault ground motions. Nat Hazards 80(3):1443–1473. https://doi.org/10.1007/s11069-015-2029-7
NTC (2018) Norme Tecniche Per Le Costruzioni. Rome, Italy
NZS 1170.5:2004 (2004) Structural Design Actions—Part 5: earthquake actions. Wellington, New Zealand
O'Reilly GJ (2021) Limitations of Sa(T 1) as an intensity measure when assessing non-ductile infilled RC frame structures. Bull Earthq Eng 19(6):2389–2417. https://doi.org/10.1007/s10518-021-01071-7
O'Reilly GJ, Calvi GM (2021) A seismic risk classification framework for non-structural elements. Bull Earthq Eng 19(13):5471–5494. https://doi.org/10.1007/s10518-021-01177-y
O'Reilly GJ, Nafeh AMB (2021) Infilled-RC-building-database. GitHub Repos. https://doi.org/10.5281/zenodo.5082990
O'Reilly GJ, Sullivan TJ (2019) Modeling techniques for the seismic assessment of the existing Italian RC Frame structures. J Earthq Eng 23(8):1262–1296. https://doi.org/10.1080/13632469.2017.1360224
O'Reilly GJ, Perrone D, Fox M, Monteiro R, Filiatrault A (2018) Seismic assessment and loss estimation of existing school buildings in Italy. Eng Struct 168:142–162. https://doi.org/10.1016/j.engstruct.2018.04.056
Ozsarac V (2022) Toolbox for ground motion selection and processing. DOI: 10.5281/zenodo.5878962
Papadopoulos AN, Vamvatsikos D, Kazantzi AK (2019) Development and application of FEMA P-58 compatible story loss functions. Earthq Spectra 35(1):95–112. https://doi.org/10.1193/102417EQS222M
Perrone D, Filiatrault A (2017) Automated seismic design of non-structural elements with building information modelling. Autom Constr 84:166–175. https://doi.org/10.1016/j.autcon.2017.09.002
Perrone G, Cardone D, O'Reilly GJ, Sullivan TJ (2022) Developing a direct approach for estimating expected annual losses of Italian buildings. J Earthq Eng 26(1):1–32. https://doi.org/10.1080/13632469.2019.1657988
Priestley MJN, Calvi GM, Kowalsky MJ (2007) Displacement Based seismic design of structures. IUSS Press, Pavia, Italy
Ramirez CM, Miranda E (2009) Building specific loss estimation methods & tools for simplified performance based earthquake engineering. Blume Report No 171
Ramirez CM, Miranda E (2012) Significance of residual drifts in building earthquake loss estimation. Earthq Eng Struct Dyn 41(11):1477–1493. https://doi.org/10.1002/eqe.2217
Rosenblueth E, Meli R (1986) The 1985 Mexico earthquake: causes and effects in Mexico City. Concr Int 8(5):23–34
Ruiz-Garcia J, Miranda E (2005) Performance-based assessment of existing structures accounting for residual displacements, Technical Report No. 153. Stanford, California
Ruiz-García J, Chora C (2015) Evaluation of approximate methods to estimate residual drift demands in steel framed buildings. Earthq Eng Struct Dyn 44(15):2837–2854. https://doi.org/10.1002/eqe.2611
Ruiz-García J, Miranda E (2006a) Residual displacement ratios for assessment of existing structures. Earthq Eng Struct Dyn 35(3):315–336. https://doi.org/10.1002/eqe.523
Ruiz-García J, Miranda E (2006b) Evaluation of residual drift demands in regular multi-storey frames for performance-based seismic assessment. Earthq Eng Struct Dyn 35(13):1609–1629. https://doi.org/10.1002/eqe.593
Sassun K, Sullivan TJ, Morandi P, Cardone D (2016) Characterising the in-plane seismic performance of infill masonry. Bull N Z Soc Earthq Eng 49(1):98–115. https://doi.org/10.5459/bnzsee.49.1.98-115
Shahnazaryan D, O'Reilly GJ, Monteiro R (2021) Story loss functions for seismic design and assessment: Development of tools and application. Earthq Spectra 37(4):2813–2839. https://doi.org/10.1177/8755293021102352 3
Shahnazaryan D, O'Reilly GJ (2023) Fitting improved hazard models for SAC/FEMA-compatible seismic analysis. In: 14th International Conference on Applications of Statistics and Probability in Civil Engineering, ICASP14, Dublin, Ireland
Silva A, Macedo L, Monteiro R, Castro JM (2020a) Earthquake-induced loss assessment of steel buildings designed to Eurocode 8. Eng Struct 208:110244. https://doi.org/10.1016/j.engstruct.2020.110244
Silva A, Castro JM, Monteiro R (2020b) A rational approach to the conversion of FEMA P-58 seismic repair costs to Europe. Earthq Spectra 36(3):1607–1618. https://doi.org/10.1177/8755293019899964
Sullivan TJ (2016) Use of limit state loss versus intensity models for simplified estimation of expected annual loss. J Earthq Eng 20(6):954–974. https://doi.org/10.1080/13632469.2015.1112325
Sullivan TJ, Calvi PM, Nascimbene R (2013) Towards improved floor spectra estimates for seismic design. Earthq Struct 4(1):109–132. https://doi.org/10.12989/eas.2013.4.1.109
Taghavi S, Miranda E (2005b) Approximate floor acceleration demands in multistory buildings. II: applications. J Struct Eng 131(2):212–220. https://doi.org/10.1061/(ASCE)0733-9445(2005)131:2(212)

Vamvatsikos D (2013) Derivation of new SAC/FEMA performance evaluation solutions with second-order hazard approximation. Earthq Eng Struct Dyn 42(8):1171–1188. https://doi.org/10.1002/eqe.2265

Vamvatsikos D, Cornell CA (2005) Direct estimation of seismic demand and capacity of multidegree-of-freedom systems through incremental dynamic analysis of single degree of freedom approximation. J Struct Eng 131(4):589–599. https://doi.org/10.1061/(asce)0733-9445(2005)131:4(589)

Vamvatsikos D, Cornell CA (2006) Direct estimation of the seismic demand and capacity of oscillators with multi-linear static pushovers through IDA. Earthq Eng Struct Dyn 35(9):1097–1117. https://doi.org/10.1002/eqe.573

Vukobratović V, Fajfar P (2015) A method for the direct determination of approximate floor response spectra for SDOF inelastic structures. Bull Earthq Eng 13(5):1405–1424. https://doi.org/10.1007/s10518-014-9667-0

Vukobratović V, Fajfar P (2016) A method for the direct estimation of floor acceleration spectra for elastic and inelastic MDOF structures. Earthq Eng Struct Dyn 45(15):2495–2511. https://doi.org/10.1002/eqe.2779

Vukobratović V, Fajfar P (2017) Code-oriented floor acceleration spectra for building structures. Bull Earthq Eng 15(7):3013–3026. https://doi.org/10.1007/s10518-016-0076-4

Welch DP, Sullivan TJ, Filiatrault A (2014a) Potential of building information modelling for seismic risk mitigation in buildings. Bull N Z Soc Earthq Eng 47(4):253–263. https://doi.org/10.5459/bnzsee.47.4.253-263

Welch DP, Sullivan TJ, Calvi GM (2014b) Developing direct displacement-based procedures for simplified loss assessment in performance-based earthquake engineering. J Earthq Eng 18(2):290–322. https://doi.org/10.1080/13632469.2013.851046

Woessner J, Laurentiu D, Giardini D, Crowley H, Cotton F, Grünthal G et al (2015) The 2013 European seismic hazard model: key components and results. Bull Earthq Eng 13(12):3553–3596. https://doi.org/10.1007/s10518-015-9795-1

Zsarnóczay Á, Deierlein GG (2020) PELICUN—a computational framework for estimating damage, loss and community resilience. In: 17th World Conference on Earthquake Engineering, Sendai, Japan

Publisher's Note Springer Nature remains neutral with regard to jurisdictional claims in published maps and institutional affiliations.

Springer Nature or its licensor (e.g. a society or other partner) holds exclusive rights to this article under a publishing agreement with the author(s) or other rightsholder(s); author self-archiving of the accepted manuscript version of this article is solely governed by the terms of such publishing agreement and applicable law.